Petroleum Science 22 (2025) 588–606

Contents lists available at ScienceDirect

Petroleum Science

journal homepage: www.keaipublishing.com/en/journals/petroleum-science

Original Paper

Restoration of hydrocarbon generation potential of the highly mature Lower Cambrian Yuertusi Formation source rocks in the Tarim Basin

Yao Hu [a, b, c, d], Cheng-Zao Jia [a, b, c, *], Jun-Qing Chen [a, e, **], Xiong-Qi Pang [a, b], Lin Jiang [a, c, d], Chen-Xi Wang [a, b], Hui-Yi Xiao [a, b], Cai-Jun Li [a, b], Yu-Jie Jin [a, b]

[a] State Key Laboratory of Petroleum Resources and Engineering, China University of Petroleum (Beijing), Beijing, 102249, China
[b] College of Geoscience, China University of Petroleum (Beijing), Beijing, 102249, China
[c] Research Institute of Petroleum Exploration and Development, PetroChina, Beijing, 100083, China
[d] CNPC Key Laboratory of Basin Structure and Hydrocarbon Accumulation, Beijing, 100083, China
[e] Basic Research Center for Energy Interdisciplinary, College of Science, China University of Petroleum (Beijing), Beijing, 102249, China

A R T I C L E I N F O

Article history:
Received 26 May 2024
Received in revised form
3 August 2024
Accepted 3 December 2024
Available online 4 December 2024

Edited by Jie Hao and Min Li

Keywords:
Evaluation of resource potential
Highly mature hydrocarbon source rocks
Yuertusi formation
Tarim Basin

A B S T R A C T

The Early Cambrian Yuertusi Formation ($Є_1y$) in the Tarim Basin of China deposits a continuously developed suite of organic-rich black mudstones, which constitute an important source of oil and gas reservoirs in the Paleozoic. However, its hydrocarbon generation and evolution characteristics and resource potential have long been constrained by deeply buried strata and previous research. In this paper, based on the newly obtained ultra-deep well drilling data, the hydrocarbon generation and expulsion model of $Є_1y$ shale was established by using data-driven Monte Carlo simulation, upon which the hydrocarbon generation, expulsion, and retention amounts were calculated by using the diagenetic method. The research indicates that the $Є_1y$ shale reaches the hydrocarbon generation and expulsion threshold at equivalent vitrinite reflectances of 0.46% and 0.72%, respectively. The cumulative hydrocarbon generation is 68.88×10^{10} t, the cumulative hydrocarbon expulsion is 35.59×10^{10} t, and the cumulative residual hydrocarbon is 33.29×10^{10} t. This paper systematically and quantitatively calculates the hydrocarbon expulsion at various key geological periods for the $Є_1y$ source rocks in the study area for the first time, more precisely confirming that the black shale of the $Є_1y$ is the most significant source rock contributing to the marine oil and gas resources in the Tarim Basin, filling the gap in hydrocarbon expulsion calculation in the study area, and providing an important basis for the formation and distribution of Paleozoic hydrocarbon reservoirs. The prospect of deep ultra-deep oil and gas exploration in the Tarim Basin is promising. Especially, the large area of dolomite reservoirs under the Cambrian salt and source rock interiors are the key breakthrough targets for the next exploration in the Tarim Basin.

1. Introduction

The Precambrian-Cambrian transition has long been recognized as a key transitional period in geologic history, during which the Earth's surface system experienced a series of major geologic events such as changes in oceanic redox conditions, the development and ablation of extensive glaciers, and the rifting and coalescence of supercontinents, which profoundly affected the evolution of eukaryotic algae and epifauna (Eigenbrode and Freeman, 2006; Canfield et al., 2007; Campbell and Allen, 2008; Erwin et al., 2011; Och et al., 2012; Lyons et al., 2014; Chen et al., 2020; Zhang et al., 2024). In the early Cambrian, the global climate changed from cold to warm, the atmospheric oxygen content increased rapidly, and the sea level rose massively, resulting in the deposition of a large area of continuously developed high-quality black shales in the East Siberia Basin, the Indus River Basin, the Oman Basin, the Tarim Basin, and the Yangtze region on both sides of the ancient Asian Ocean (Terken et al., 2001; Grosjean et al., 2009; Craig et al., 2013; Liu et al., 2024). They not only preserve key geological information for understanding the co-evolution of early Earth's environmental changes and life but also

* Corresponding author.
** Corresponding author.
E-mail addresses: jiacz@petrochina.com.cn (C.-Z. Jia), cjq7745@163.com (J.-Q. Chen).

https://doi.org/10.1016/j.petsci.2024.12.001
1995-8226/

serve as essential sources of hydrocarbon supply for the Paleozoic reservoirs in the aforementioned areas (Zhu et al., 2018, 2019a). The Early Cambrian black shale of the Yuertusi Formation ($Є_1y$), deposited in the Tarim Basin (TB) of China, is considered to be the most excellent marine source rock discovered in China and has attracted widespread attention for its high total organic carbon (TOC) content, wide distribution area, and high hydrocarbon potential (Zhu et al., 2018; Li et al., 2023).

A vast amount of research has been conducted on the $Є_1y$ shale, especially on their geochemistry, and rich results have been obtained in the areas of paleostratigraphy, sedimentary paleoenvironmental restoration, source of hydrocarbon parent material, thickness prediction, organic matter (OM) thermal evolution, and distribution and development patterns (Hu et al., 2018, 2022; Zhu et al., 2018; Fan et al., 2020; He et al., 2020a, 2020b, 2022; Gao et al., 2022; Li et al., 2022, 2023; Zhao et al., 2023). Based on outcrop, seismic, and drilling data, previous studies suggest that the distribution of the $Є_1y$ source rocks is controlled by the paleotopographic rift valleys of the late Ediacaran. The black siliceous shale formed under anoxic conditions in the Tabei slope area is of the best quality, with high TOC content and abundant petroleum reserves (Zhu et al., 2020; Wu et al., 2021; Yuan et al., 2022). According to seismic facies data, many scholars have predicted the distribution of Cambrian source rocks. Despite differences in thickness and distribution area, it has become widely accepted that the $Є_1y$ source rocks are extensively distributed in the southern Tabei Uplift, Manjiaer Depression, eastern Awati Depression, and Maigaiti Slope (Yang et al., 2017; Zhu et al., 2018; Wang et al., 2024). Gao et al. (2022) analyzed the depositional environment and distribution of the $Є_1y$ source rocks using outcrop sections, drilling, and seismic data, dividing them into two third-order sequences and five fourth-order sequences, and suggested that sq2 and sq4, formed during transgressive periods, have the highest TOC content and substantial resources. Deng et al. (2021) studied the depositional environment and OM differentiation mechanisms of the lower Cambrian strata in the western and northeastern Tarim Basin by analyzing the geochemical characteristics of field outcrops. Regarding the resource potential of $Є_1y$, scholars, and institutions have conducted studies and preliminary assessments. Zhang et al. (2022) calculated that the oil and gas resources of the Cambrian source rocks, including $Є_1y$, are approximately 75×10^{10} t of oil equivalent. The USGS (United States Geological Survey, 2018) estimated the technically recoverable shale gas resources of $Є_1y$ to be about 45.91×10^{10} m^3 based on geological assessment methods (Potter et al., 2019). However, research on the hydrocarbon generation (HG) and hydrocarbon expulsion (HE) characteristics and resource potential of the $Є_1y$ source rocks is still relatively weak and lacks systematic work, and whether its HG capacity and resource potential can satisfy the reservoir size of deep Paleozoic reservoirs in the TB has not yet been clarified (Handson et al., 2000; Sun et al., 2003; Li et al., 2010; Zhu et al., 2018). There are two main problems, one is that the Cambrian stratum has a great depth, resulting in a limited number of actually drilled source rock samples of the $Є_1y$, and the necessary basic parameters such as OM abundance, thickness, and distribution area are limited. Previously, a small number of drill and field outcrop samples were typically utilized, resulting in insufficient evaluation accuracy and the need to incorporate the latest information. Secondly, it is difficult to obtain low-maturity samples from the $Є_1y$, making it difficult to establish HG and HE models for source rocks using conventional methods such as thermal simulation experiments and basin simulations (Peters et al., 2015; Li et al., 2020, 2021a). Pang et al. (2005) proposed the hydrocarbon generation potential method (HGPM) based on the material balance principle, which can quantitatively evaluate the HG and HE characteristics of source rocks in geological history and effectively avoid the above problems. Subsequently, scholars continuously improved and applied this method to shallow and deep source rock formations in various basins (Zheng et al., 2019; Li et al., 2020, 2021a; Wang et al., 2022), confirming the reliability of this method. In addition, a series of ultra-deep drilling operations, such as QT 1 well in 2019, LN 1 well in 2020, and LT 3 well in 2021, have successively encountered hydrocarbon source rock samples from $Є_1y$. Many scientists have conducted extensive geochemical analysis work on the Cambrian samples from LT 1 well (Yang et al., 2020a; Zhu et al., 2021, 2022), which provides rare data for evaluation in this study.

Based on the fundamental work of predecessors, this study systematically summarized the characteristics of the $Є_1y$ source rocks by collecting data from 11 wells and 6 outcrop profiles in the TB. Meanwhile, the hydrocarbon potential method (Li et al., 2020) was applied to establish the HG and HE model of $Є_1y$, the hydrocarbon history was recovered, and the amount of HG and HE during the key geological history was calculated, which further clarified the resource potential of $Є_1y$ in the TB. The above research findings based on the latest geological data provide a geological foundation for the exploration of deep hydrocarbon resources in the TB.

2. Geological background

The TB, situated in the south of Xinjiang, China, is a superimposed composite basin formed in the context of the Precambrian paleocraton sandwiched between the Tianshan Mountains, Kunlun Mountains, and Altun Mountains. It is also the largest marine petroliferous basin and oil production base in inland China, with a total area of 56×10^4 km^2 (Yang et al., 2016b). The basin has experienced complex multi-phase tectonic movements and superimposed evolution, with seven tectonic movements forming the current structural unit of the “five uplifts and five depressions" (Pang et al., 2012b). The five uplifts are Tabei Uplift, Tazhong Uplift, Bachu Uplift, Tadong Uplift, and Keping Fault Uplift, respectively. The five depressions are composed of Kuqa Depression, Northern Depression, Southwest Depression, Tanggu Depression, and Southeast Depression (Liu et al., 2016a; He et al., 2022). The Kuqa Depression, Northern Depression, and Southeastern Depression are foreland basin areas of the Meso-Cenozoic era at the basin periphery, while the remaining structural units belong to the craton area of the basin. These primary structural units can be further subdivided into secondary structural units, such as the Northern Depression, which can be further divided into the Manjiaer Depression, Awati Depression, and so on (Fig. 1).

The TB has a complete Taikonian-Early Neoproterozoic cratonic crystalline basement, on which Neoproterozoic-Cenozoic marine, marine-land transitional, and terrestrial strata were deposited sequentially. The Ediacaran to Silurian mainly deposited marine strata, of which the Ediacaran and Silurian mainly developed marine clastic rocks, while the Cambrian-Ordovician was mainly dominated by carbonate rocks. The Devonian-Permian was a period of mutual deposition of land and sea. After the Triassic, the TB entered a period of terrestrial clastic deposition and development (He et al., 2005). Cambrian-Ordovician carbonate formations are spread throughout the basin and are the focus of exploration in the TB (Zhu et al., 2019b, Fig. 2). During the deposition of the $Є_1y$, global sea levels rose rapidly, creating a suite of excellent hydrocarbon source rocks (Sun et al., 2004; Chen et al., 2017; He et al., 2020a). However, the thickness varies depending on the depositional environment. The depositional environment of $Є_1y$ shales in the eastern Tarim and western Tarim could be very different. The $Є_1y$ shales in the eastern Tarim were primarily deposited in basinal

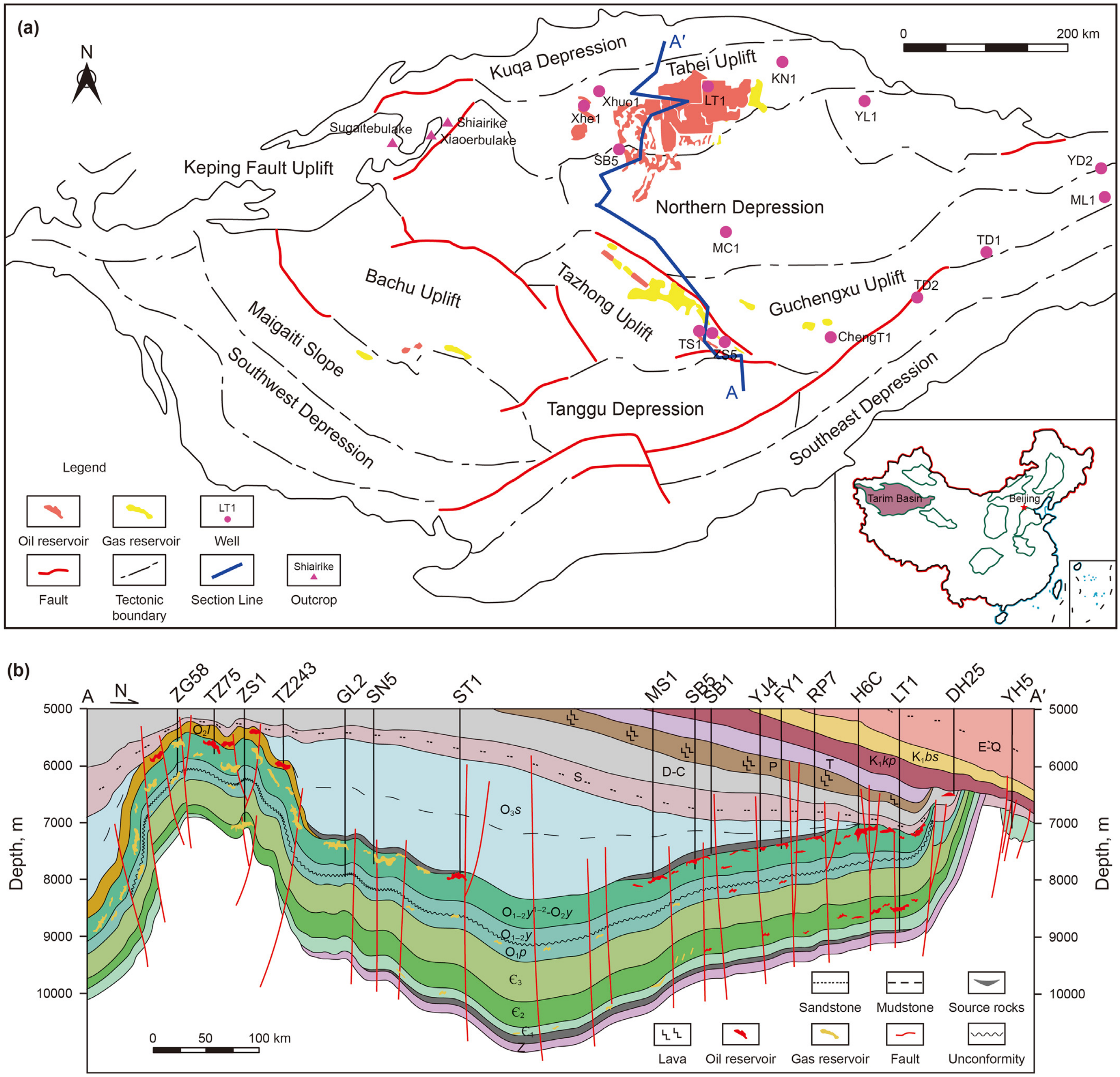

Fig. 1. **(a)** Tectonic units of the TB (Modified after Zhu et al. (2019b)). **(b)** The reservoir profile with S-N direction across the basin (Location as shown in Fig. 1(a); modified after Jia and Zhang (2023)).

facies/deep water settings, where the source rocks have considerable thickness (greater than 50 m) (Xiong et al., 2015; Zhu et al., 2020; Deng et al., 2021), while the $Є_1y$ shales in the western Tarim were mainly deposited in slope shelf facies, where the source rock thickness is relatively thinner (Zhu et al., 2018). The lower section of the $Є_1y$ is mainly developed by black phosphorus-bearing siliceous rocks, black shale, and phosphate block rocks, with a thickness of about 20 m; the upper section is dominated by dolomite limestone, totaling 15–50 m in thickness (Yang et al., 2020a; Zhu et al., 2022). Relatively complete $Є_1y$ sections (such as the Kungaikuotan section and the Sugaitebulake section) are exposed in the Keping area.

3. Data and methods

3.1. Data sources

The depth of the Cambrian strata makes it challenging to conduct exploration drilling into the area. Furthermore, obtaining actual geological samples is difficult for limited wells that have been drilled into the region. The majority of research is conducted based on field outcrop profiles and predicted data from related studies. A portion of the data for this study was obtained from the Tarim Oilfield, while the remainder was derived from previous studies (Feng and Chen, 1988; Liu et al.,1999; Liu, 2015; Liu et al., 2016b; Wang, 2019; Deng, 2021; Xue, 2021; Zhou, 2021). To

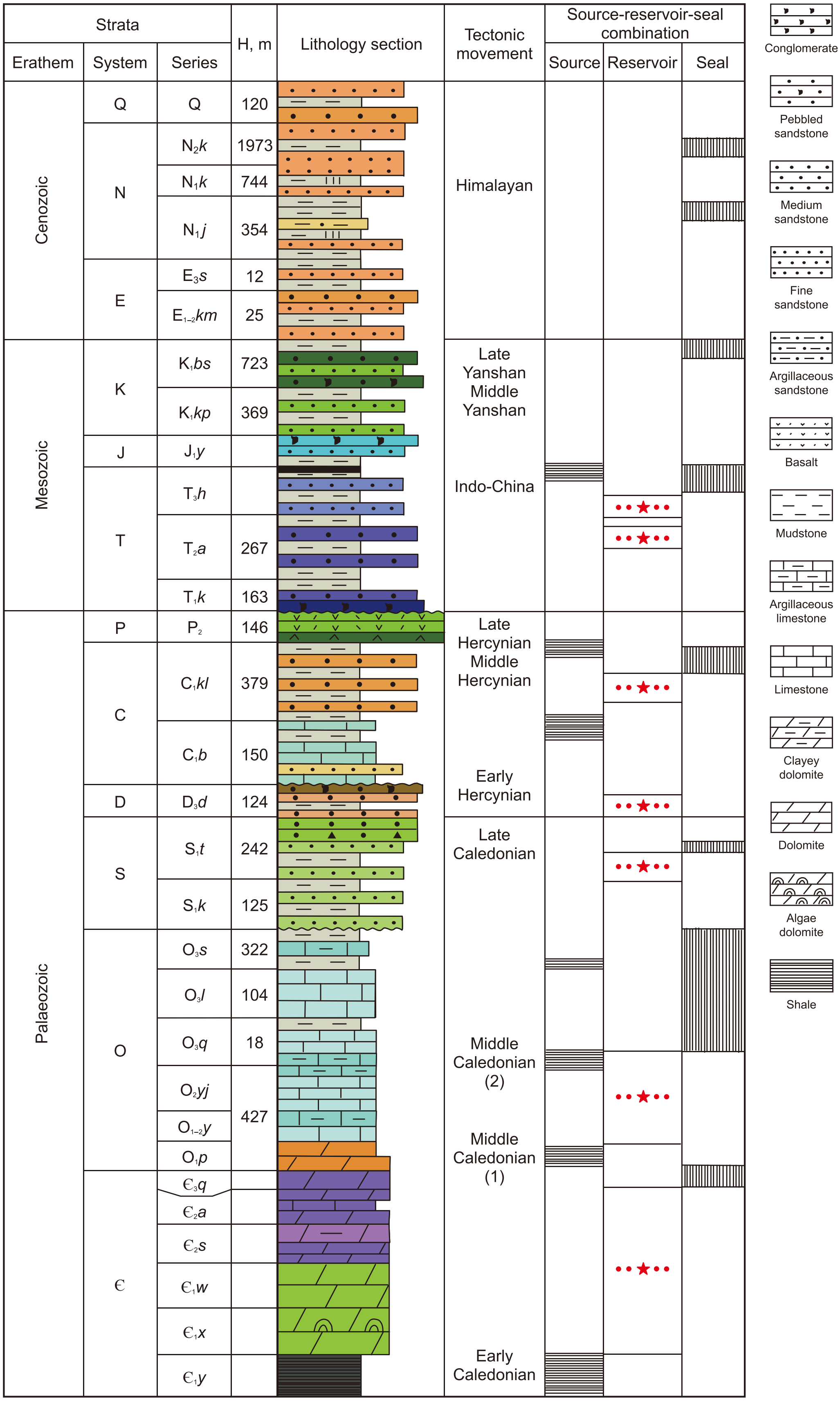

Fig. 2. Stratigraphic column of the Tarim Basin (Modified after Zhu et al. (2019b)).

ensure the reliability of the research results, a sufficient number of samples were collected for analysis. The samples encompass the majority of the shales that have been developed in a variety of tectonic zones, at varying burial depths, and within diverse sedimentary environments within the TB. The pyrolysis parameters, including S_1 and S_2, as well as TOC and equivalent vitrinite reflectance ($R_{eq.}$), were sourced from 65 data points of the LT1 (Yang et al., 2020a; Zhu et al., 2022). The data utilized to analyze the geological and geochemical characteristics encompass 124 data from LT 1 and 223 data from six exploration wells in the Tadong area (TD 1, TD 2, ML 1, GC 2, YD 2, and KN 1), totaling 347 data. The remaining parameters include source rock thickness, OM content, OM maturity, and rock density. The thickness map of the source rock was derived from Zhu et al. (2018). The distribution map of OM maturity was obtained from the Tarim Oilfield. The source rocks density values were selected from Li et al. (2021c).

3.2. Conceptual model of hydrocarbon generation and expulsion

The HGPM is founded upon the principles of material conservation and the theory of hydrocarbon expulsion threshold (HET) (Pang et al., 2005), characterized by convenience and effectiveness. The hydrocarbon model of the source rock of the target layer is established in the process of geological history, and its HG and HE processes are quantitatively characterized and evaluated for resource potential. This is illustrated in Fig. 3.

The OM in source rocks includes residual OM that has not yet been converted into oil and gas, hydrocarbons that have been generated and remain in the source rocks (HCI), and hydrocarbons that have been expelled from the source rocks (Q_e). The principle of conservation of matter suggests that the total mass of the three remains unchanged during their thermal evolution. The variation patterns of the hydrocarbon generation potential index (GPI, Zhou and Pang (2002)) and hydrogen index (HI) on the thermal evolution profile are employed to characterize the HG and HE characteristics. S_1 represents the hydrocarbons evaporated when the rock sample is heated up to 300 °C, while S_2 represents the hydrocarbons generated by high-temperature rock samples at temperatures ranging from 300 °C to 600 °C. Before HG, the HI of the source rock remains unaltered, representing the original hydrogen index (HI_o). After the generation of hydrocarbons, the HI gradually decreases; When the source rock only generates hydrocarbons without expelling them, the GPI remains unchanged, representing the original GPI (GPI_o). Subsequently, the GPI_o gradually decreases following the expulsion of hydrocarbons. Consequently, the $R_{eq.}$ corresponding to the point where the HI begins to decrease and the transformation rate (T_R) begins to increase is the hydrocarbon generation threshold (HGT). The $R_{eq.}$ corresponding to the point where the *GPI* begins to decrease and the hydrocarbon expulsion ratio (E_R) begins to increase is the hydrocarbon expulsion threshold (HET). The $R_{eq.}$ corresponding to the peak of the hydrocarbon generation rate (R_G) and hydrocarbon expulsion rate (R_E) is the peak of HG and HE, respectively. The E_R is expressed as the ratio of the HE mass to its maximum HG potential mass (Eq. (1)), representing the HE degree. T_R represents the degree of OM thermal degradation, expressed by Eq. (2). The value of E_R to T_R represents the efficiency of HE (f) (Eq. (3)). The RG and RE are represented by the derivatives of (HI_o-HI) and (GPI_o-GPI), respectively, representing the changes in the HG rate (or amount) and HE rate (or amount) of the source rock within a unit geological history period or unit burial depth (or degree of evolution), as determined by Eqs. (4) and (5). Rock quality and organic carbon loss occur in the process of maturation of source rocks, therefore both need to be restored. This study utilizes Eqs. (6) and (7) to calculate the rock mass recovery coefficients (φ) corresponding to each mature stage and original TOC (TOC_o) (Jiang et al., 2015; Li et al., 2020). Based on the above parameters, according to Eqs. (8)–(13), the intensity of HG (I_g), intensity of HE (I_e), intensity of HR (I_r), quantity of HG (Q_g), quantity of HE (Q_e), and quantity of HR (Q_r) can be determined for each geological period (More detailed description on this model could be seen in Li et al., 2020).

$$E_R = \frac{1000\alpha \times (GPI_o - GPI)}{GPI_o \times (1000\alpha - GPI)} \tag{1}$$

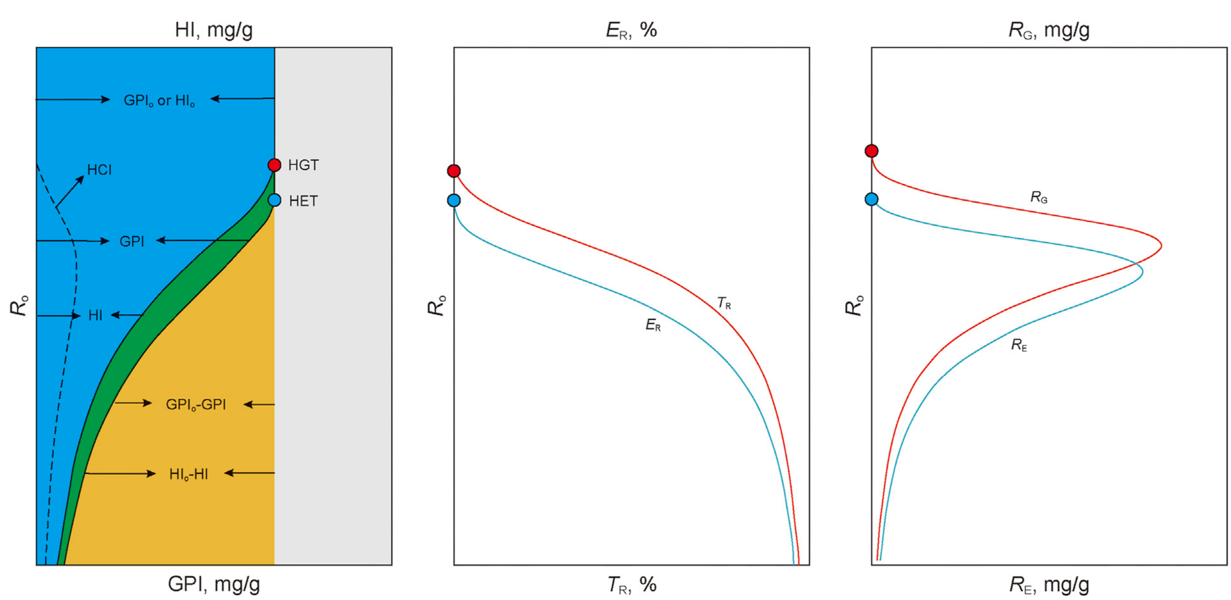

Fig. 3. The comprehensive conceptual model of hydrocarbon generation and expulsion potential method (HCI: hydrocarbon index; HI: hydrogen index; GPI: hydrocarbon generation potential index; HI_o: original hydrogen index; GPI_o: original hydrocarbon generation potential index; HGT: hydrocarbon generation threshold; HET: hydrocarbon expulsion threshold; E_R: hydrocarbon expulsion ratio; T_R: transformation rate; R_G: hydrocarbon generation rate; R_E: hydrocarbon expulsion rate; Li et al., 2020).

$$T_R = \frac{HI_o \times (1000\alpha - HCI) - (1000\alpha \times HI)}{HI_o \times (1000\alpha - HI - HCI)} \tag{2}$$

$$f = \frac{E_R}{T_R} \tag{3}$$

$$R_G(R_o) = \frac{dHI}{dR_o} \tag{4}$$

$$R_E(R_o) = \frac{dGPI}{dR_o} \tag{5}$$

$$\varphi = \left(1 - \frac{GPI_o}{1000} \times \frac{TOC_o}{100} \times E_R\right)^{-1} \tag{6}$$

$$TOC_o = \frac{TOC}{1 - \frac{GPI_o}{1000\alpha} \times E_R \times \left(1 - \alpha \times \frac{TOC}{100}\right)} \tag{7}$$

$$I_g = \int_{HGT}^{R_o} 10^{-3} \cdot HI_o \cdot H \cdot \rho \cdot TOC_o(R_o) \cdot \varphi(R_o) \cdot T_R(R_o) \cdot d(R_o) \tag{8}$$

$$I_e = \int_{HGT}^{R_o} 10^{-3} \cdot GPI_o \cdot H \cdot \rho \cdot TOC_o(R_o) \cdot \varphi(R_o) \cdot E_R(R_o) \cdot d(R_o) \tag{9}$$

$$I_r = \int_{HGT}^{R_o} 10^{-3} \cdot GPI_o \cdot H \cdot \rho \cdot TOC_o(R_o) \cdot \varphi(R_o) \cdot (T_R(R_o) - E_R(R_o)) \cdot d(R_o) \tag{10}$$

$$Q_g = \int_{HGT}^{R_o} 10^{-3} \cdot HI_o \cdot H \cdot S \cdot \rho \cdot TOC_o(R_o) \cdot \varphi(R_o) \cdot T_R(R_o) \cdot d(R_o) \tag{11}$$

$$Q_e = \int_{HGT}^{R_o} 10^{-3} \cdot HI_o \cdot H \cdot S \cdot \rho \cdot TOC_o(R_o) \cdot \varphi(R_o) \cdot E_R(R_o) \cdot d(R_o) \tag{12}$$

$$Q_r = \int_{HGT}^{R_o} 10^{-3} \cdot GPI_o \cdot H \cdot S \cdot \rho \cdot TOC_o(R_o) \cdot \varphi(R_o) \cdot (T_R(R_o) - E_R(R_o)) \cdot d(R_o) \tag{13}$$

where E_R is the hydrocarbon expulsion rate, %; T_R is the conversion rate, %; GPI_o is the original hydrocarbon generation potential index, mg HC/g TOC; HI_o is the original hydrogen index, mg HC/g TOC; R_G and R_E are the rates of hydrocarbon generation and expulsion, respectively, (mg HC/g TOC)/(0.1% R_o); TOC is the measured total organic carbon, %; TOC_o is the original total organic carbon, %; φ is the original stone quality recovery coefficient, dimensionless; HGT is the hydrocarbon generation threshold, %; HET is the hydrocarbon expulsion threshold, %; H is the thickness of the source rock, m; ρ is the density of the source rock, g/cm^3; S is the area of the source rock, m^2; I_g, I_e, and I_r respectively represent hydrocarbon generation intensity, hydrocarbon expulsion intensity, and residual hydrocarbon intensity, 10^4 t/km^2; Q_g, Q_e, and Q_r represent the hydrocarbon generation, expulsion, and residual hydrocarbon amounts, respectively, 10^8 t.

4. Results

4.1. Development and distribution characteristics of the $Є_1y$ source rocks

The $Є_1y$ in the TB belong to the Lower Cambrian Terreneuvian (Xiao et al., 2016; Zhu et al., 2019c), and are extensively distributed in the Shuntuoguole Low Uplift, Manjiaer Depression, and Awati Depression. The Tazhong Uplift is locally developed, but the thickness is relatively small and barely developed in the Bachu Uplift (developed in the Xishanbulake Formation in the Manjiaer Depression and Tadong area, both of which are isochronous deposits. The following are included in the discussion of the $Є_1y$). The sedimentation of $Є_1y$ has a wide range of upper, middle, and lower ramp, and deep-water basin facies deposits, mainly composed of mudstone, carbonaceous mudstone, and siliceous shale (Zhu et al., 2018). The majority of the Awati Depression-Tabei Uplift-Shuntuoguole Low Uplift-the west of Guchengxu and Manjiaer Depression areas are developed in all ramp facies, with the thickness of source rocks ranging from 10 to 60 m. The thickness is 12–26 m in the Akesu-Keping, about 30 m in the Tabei area, and 50–120 m in the eastern part of the Manjiaer Depression. The $Є_1y$ shale gradually thinned from the depression to the ancient uplift area and pinched out in the Bachu and Tazhong areas. The inclined area of the ancient uplift is dominated by tidal flats, with thin source rocks of 0–10 m and low TOC content. The thickness of the Southwestern Depression is relatively small, ranging from 5 to 20 m (Fig. 4).

4.2. Geochemical characteristics of source rocks in the $Є_1y$

4.2.1. OM abundance

The TOC values of 308 samples of $Є_1y$ were calculated (Table S1; Fig. 5(b)). The distribution range of TOC is 0.04%–29.78% (average: 2.50%). Specifically, 181 samples have a TOC greater than 1%, with 121 samples falling within the range of 1%–4%. The distribution range of S_1+S_2 values varies greatly, fluctuating between 0.03 and 29.08 mg/g (average: 2.01 mg/g). According to the evaluation criteria of source rocks proposed by Peters (1986) and Katz (2001), the correlation between TOC and S_1+S_2 (Fig. 5(a)) can be concluded that more than 70% of the samples of the $Є_1y$ shales are within the range of fair and high quality, indicating the $Є_1y$ source rocks are of good quality.

In this study, the TOC content contours of the $Є_1y$ shales were plotted by drilling and outcrop data based on previous studies (Pang et al., 2012b; Ge and Li, 2014; Yang et al., 2016a; Han, 2017, Fig. 6). The distribution range of TOC is relatively broad. The TOC content in the thicker Tadong area is primarily distributed within the range of 1%–3%, in the Akesu-Keping area is greater than 4%, while in the northern Tabei area is 3%–9%. In the Tadong area, the increased input of terrestrial inorganic detritus during the depositional process led to a reduction in organic matter content and decreased degradation of planktonic algae. Additionally, hydrothermal activities caused significant damage to the source rocks, resulting in lower TOC content. In contrast, the Keping and Tabei areas, which have favorable conditions for high productivity and anoxia, exhibit higher TOC content compared to the Tadong area (Zhu et al., 2020; Deng et al., 2021; Wu et al., 2021).

4.2.2. OM thermal maturity

The OM thermal maturity represents its level of thermal evolution towards hydrocarbons and is one of the most fundamental parameters for evaluating source rocks (Hartkopf et al., 2015). Many parameters are indicative of the maturity of OM, including R_o, pyrolysis parameter T_{max}, and biomarker parameters (Peters et al.,

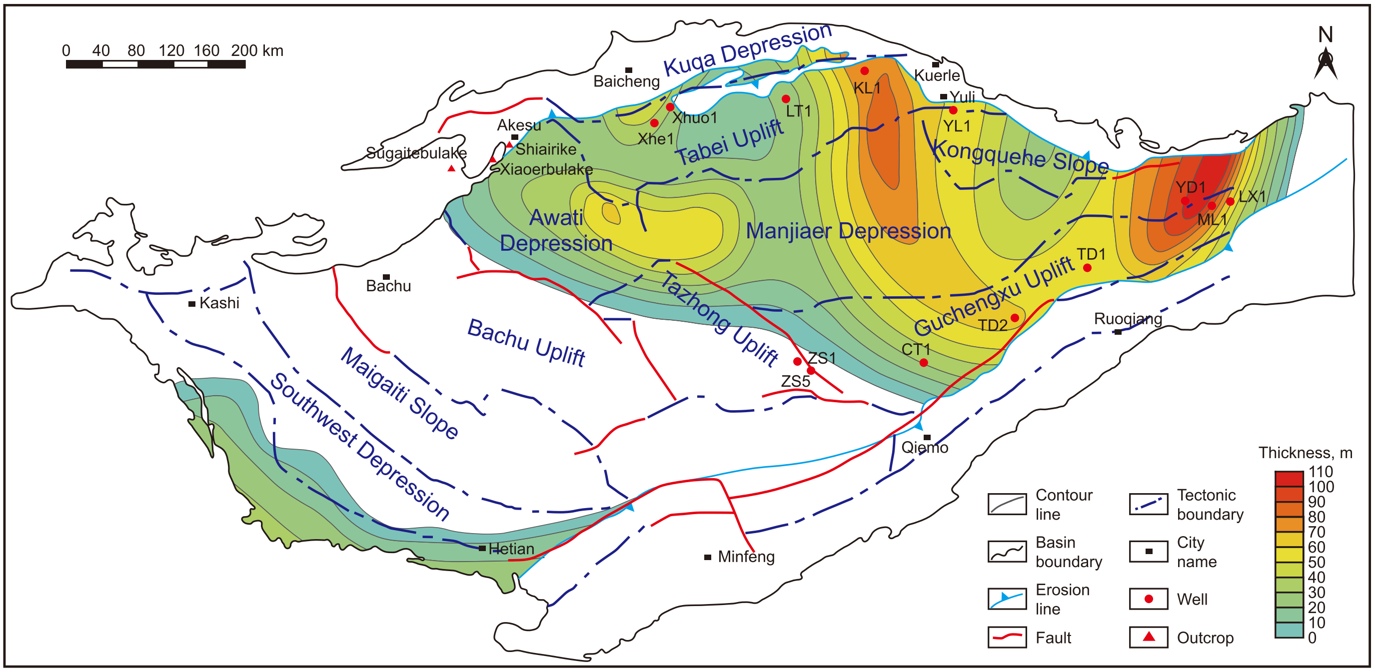

Fig. 4. Thickness distribution characteristics of the $\epsilon_1 y$ shales in the TB (Modified after Zhu et al. (2018)).

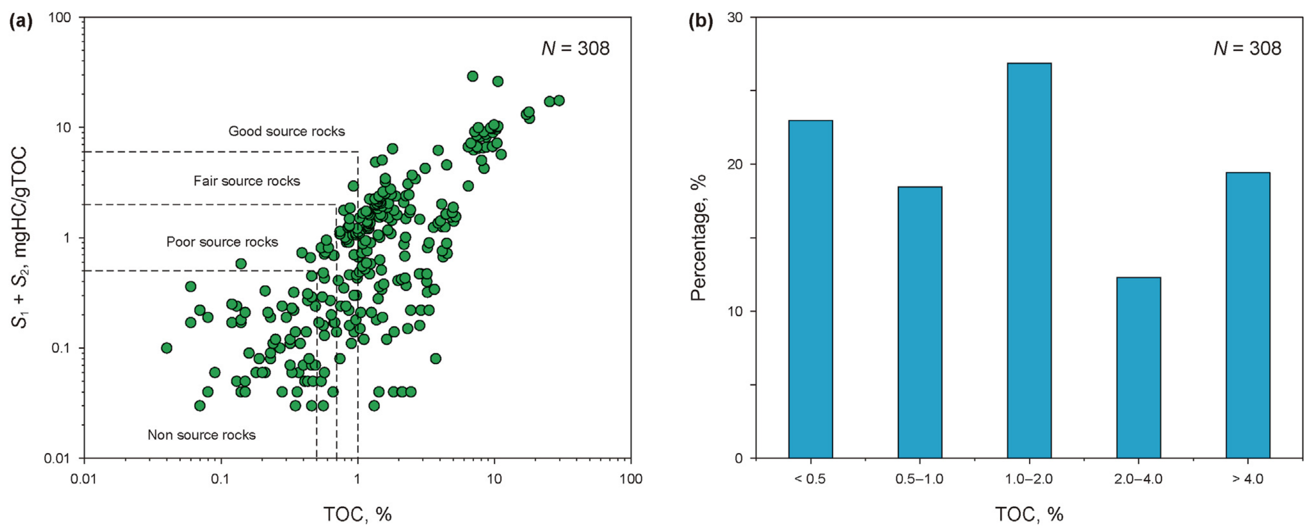

Fig. 5. Geochemical analysis of the $\epsilon_1 y$ source rocks in the TB (Modified after Peters (1986) and Katz (2001)).

2005; Burton et al., 2018; Thompson et al., 2019). R_o is widely utilized because it provides the most direct information. The $R_{eq.}$ of 57 samples of $\epsilon_1 y$ ranges from 0.98% to 2.95%, with most concentrated in the range of 1.1%–1.7% (Fig. 7(a); Table S2). The $R_{eq.}$ data indicates the $\epsilon_1 y$ samples have generally reached a high maturity - over-maturity stage. The TB has undergone three major tectonic transformations, accompanied by differential subsidence of the basin structure. Different structural units have undergone different geological evolution processes, forming the “uplift and depression" tectonic pattern of the TB, which ultimately led to the differences in the maturity of the $\epsilon_1 y$ shales between the uplift and depression units of the TB (Fig. 7(b); Zhang et al., 2022). The maturity level of the depression area is relatively high, and the $R_{eq.}$ of OM in most areas such as Manjiaer Depression, and Awati Depression is greater than 2.0%, with the highest reaching over 3.0%, so the source rock itself has lost the ability to provide large-scale hydrocarbons (Fig. 8). The source rocks in the slope area are generally more than 2000 m shallower than those in the same period in the depression area. The tectonic subsidence is relatively slow, and the $R_{eq.}$ is generally less than 2.0%. Currently, they remain in the medium to high maturity stage (Jia and Zhang, 2023).

4.2.3. OM type

OM type is an essential index for the assessment of the HG potential of source rocks. The content of hydrogen-rich components varies among different OM types, resulting in disparate hydrocarbon potentials and determining the quality of source rocks. Currently, microscopic component analysis, rock pyrolysis data, elemental analysis, kerogen type index (T-index method), and kerogen carbon isotope ($\delta^{13}C_{kerogen}$) method are commonly used to

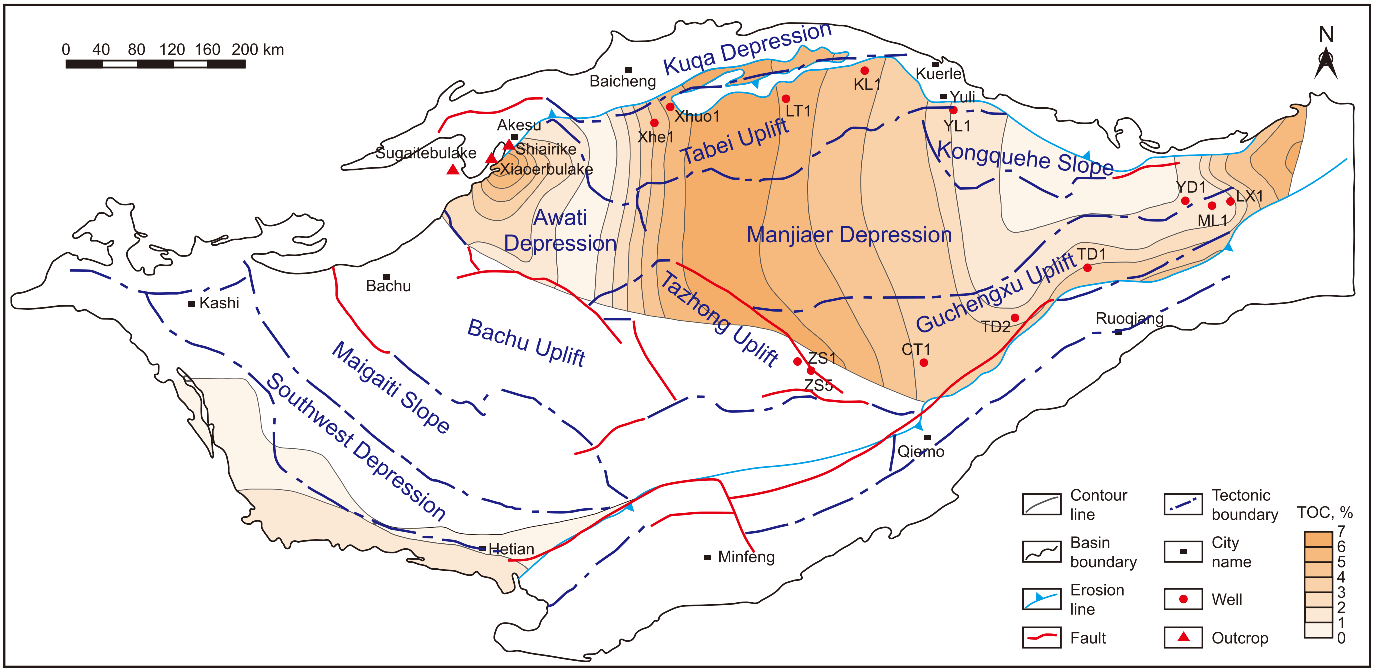

Fig. 6. TOC distribution characteristics of the ϵ_1y source rocks in the TB.

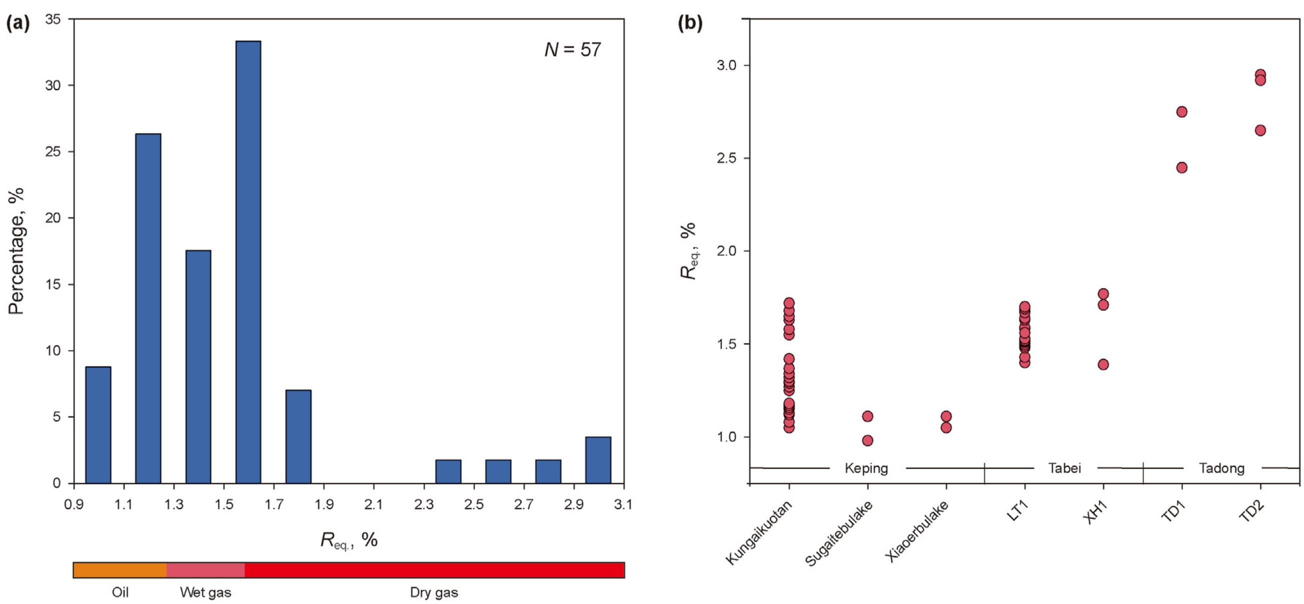

Fig. 7. Identification of thermal maturity of OM of the ϵ_1y source rocks in the TB. **(a)** Histogram of $R_{eq.}$ distribution (Tissot and Welte, 1984). **(b)** Distribution of equivalent vitrinite reflectance.

classify OM types (Katz, 1983; Peters, 1986; Peters and Cassa, 1994; Hunt, 1995). Most of the hydrocarbons generated by ϵ_1y under very high temperatures and pressures and deep-buried conditions have been turned into cracked oils and cracked gases, with hydrogen and carbon atoms greatly reduced and oxygen atom ratio increased, and the rock pyrolysis parameters cannot truly reflect the original kerogen properties (Peters et al., 2005). Nevertheless, the $\delta^{13}C_{kerogen}$ is relatively resistant to thermal maturation (Hu et al., 2018a). Furthermore, Chen et al. (2016) proposed a new cross-plot utilizing dimensionless TOC and dimensionless S_2, which effectively eliminates the effect of maturity on pyrolysis parameters. Consequently, the $\delta^{13}C_{kerogen}$ method and the cross-plot of dimensionless TOC and dimensionless S_2 are employed to evaluate the OM type of the ϵ_1y source rocks. The $\delta^{13}C_{kerogen}$ in different regions is shown in Fig. 9. The ϵ_1y source rocks exhibit a relatively light $\delta^{13}C_{kerogen}$ composition and strong heterogeneity. The $\delta^{13}C_{kerogen}$ is distributed between −24.5 ‰ and −38.6 ‰ (Table S3), with a concentration in the range −30.5 ‰ ~ −36 ‰ (average value −33.23 ‰) (Zhu et al., 2021). This isotopic composition is comparable to that of global Cambrian source rocks (Grosjean et al., 2009; Parfenova et al., 2010; Guo et al., 2011), as well as the ultra-deep crude oil in the Tabei and Maigaiti areas, suggesting that the ϵ_1y source rocks contribute to

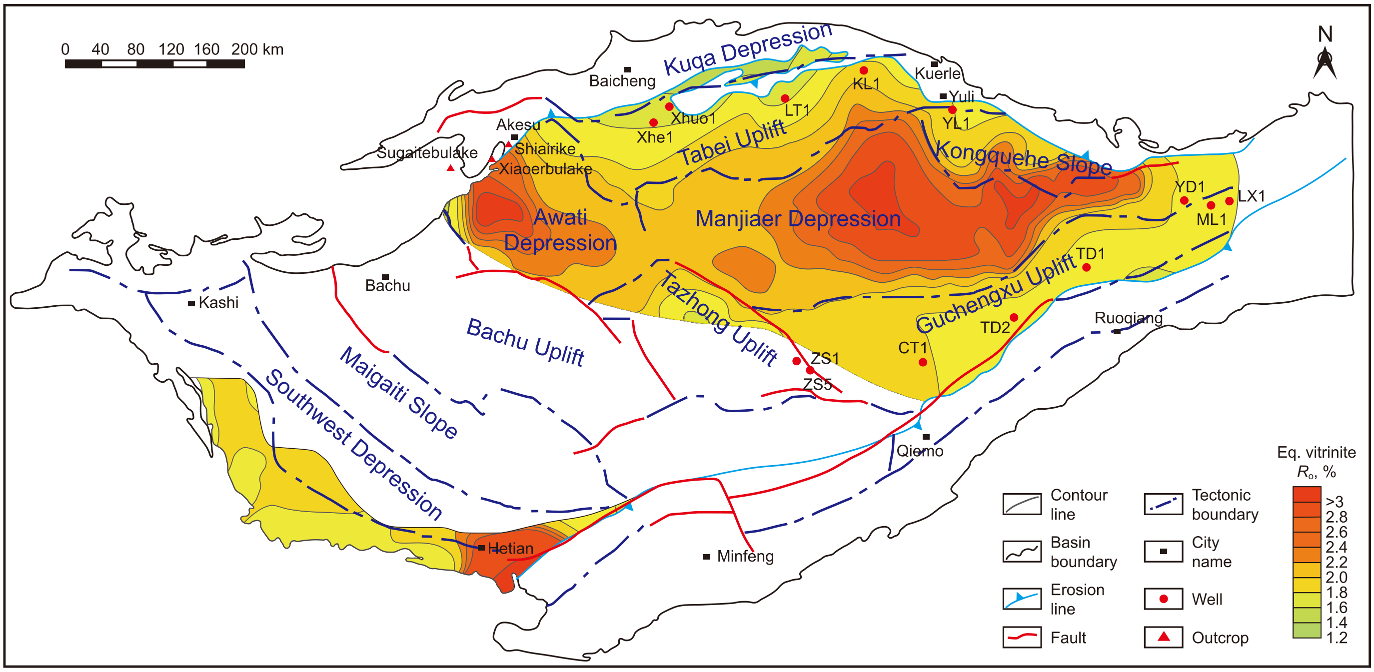

Fig. 8. Current $R_{eq.}$ distribution of the Є$_1y$ source rocks in the TB.

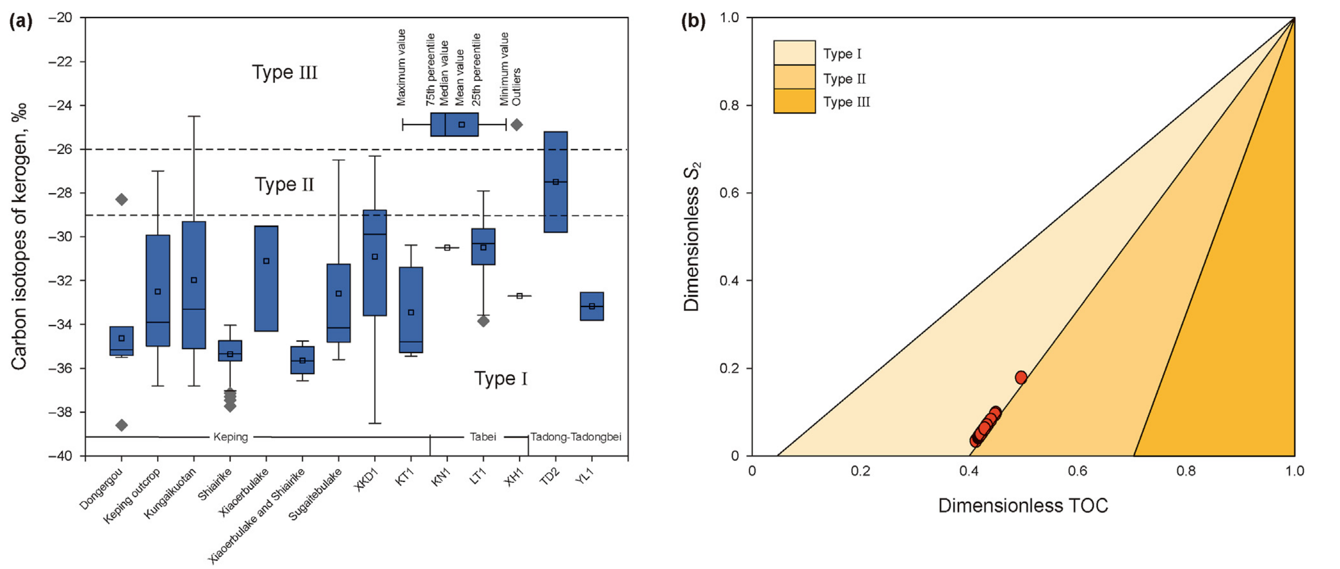

Fig. 9. Organic matter type of Є$_1y$ shale in the Tarim Basin. **(a)** The Box-and-whisker plots of $\delta^{13}C_{kerogen}$ showing Є$_1y$ shale are mainly Type I kerogen. **(b)** Dimensionless S_2 vs. TOC plot indicating Є$_1y$ shale isType I kerogen (Modified after Chen et al. (2016).

ultra-deep hydrocarbons in the TB. The $\delta^{13}C_{kerogen}$ in the western Keping area is the lightest (−24.5 ‰ ~ −38.6 ‰, average −33.66 ‰), followed by XH 1 and WL 1 (−32.54 ‰ ~ −33.8 ‰, average −33.02 ‰). LT 1 ranges from −27.9 ‰ ~ −33.84 ‰, average of −30.49 ‰ (Yang et al., 2020a; Zhu et al., 2022), while TD 2 and KN 1 are generally heavier than −31‰ (Zhu et al., 2019d). According to the standard for classifying OM types in marine source rocks based on $\delta^{13}C_{kerogen}$, the majority of $\delta^{13}C_{kerogen}$ of the Є$_1y$ source rocks are less than −29 ‰ (Type I), while a few are between −26 ‰ and −29 ‰ (Type II). Only a few samples have $\delta^{13}C_{kerogen}$ values greater than −26 ‰ (Type III). The cross plot of dimensionless TOC and dimensionless S_2 also shows that all shale samples from Є$_1y$ are type I kerogen. Consequently, a comprehensive evaluation of the Є$_1y$ indicates that the predominant OM type is Type I.

4.3. Characteristics of hydrocarbon generation and expulsion of the Є$_1y$ source rocks

4.3.1. Establishment of hydrocarbon generation and expulsion models

Based on the pyrolysis data of the Є$_1y$ samples, this study established the HG and HE model of the Є$_1y$ in the TB. The measured rock pyrolysis data revealed a correlation between GPI, HI, and $R_{eq.}$, which was subsequently fitted by the Monte Carlo method (Fig. 10). The correlation coefficient between GPI and $R_{eq.}$ was 0.46, while that between HI and $R_{eq.}$ was 0.68, indicating a

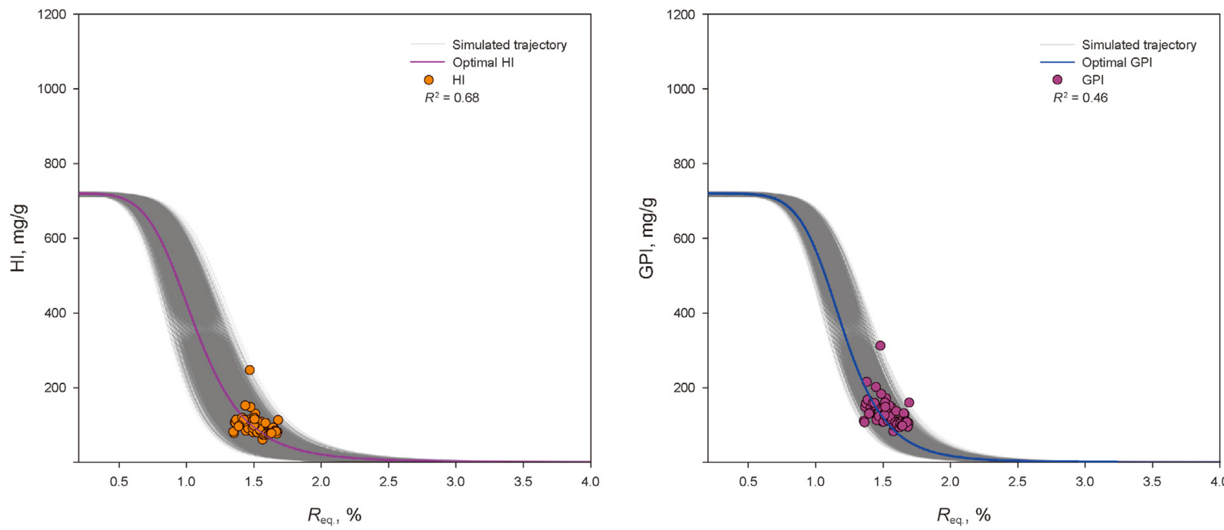

Fig. 10. Monte Carlo simulation model of HG and HE characteristics of the Є$_1y$ shale in the TB (Optimal HI: The relationship between the hydrogen index and vitrinite reflectance derived from 10000 simulations using the Monte Carlo method. Optimal GPI: The relationship between the generation potential index and vitrinite reflectance derived from 10000 simulations using the Monte Carlo method. For a more detailed explanation of this method, see Li et al. (2020).

strong correlation. An HG and HE model of the Є$_1y$ source rocks was established based on the fitting results (Fig. 11). The results indicate that the Є$_1y$ source rocks enter the HGT when the $R_{eq.}$ is approximately 0.46%. At this juncture, the quantity of hydrocarbon generated by the source rock is insufficient to meet its own needs, thus preventing any HE. Upon reaching 0.72%, the source rock enters the HET, initiating the expulsion of a considerable quantity of hydrocarbons, in accordance with the GPI_o of 716.32 mg/g. When the $R_{eq.}$ is 1.1% and 1.3%, the RG and RE reach their maximum at 839 mg/g and 1091 mg/g, respectively, signifying the peak period of HG and HE in the source rock. The average HE efficiency of the Є$_1y$ source rocks is 73%.

4.3.2. Characteristics and history of hydrocarbon generation and expulsion

The HG and HE model of the Є$_1y$ source rocks in the TB can reflect the characteristics of HG and HE in the process of maturation (Pang et al., 2005; Li et al., 2020; Wang et al., 2022; Hui et al., 2024). Previous research has identified five key periods in the maturation of the Є$_1y$ source rocks and the charging of major oil and gas fields, including the Tahe Oilfield, Lunnan Oilfield, Tazhong Oilfield, which are the late Caledonian, early Hercynian, late Hercynian, late Yanshanian, and Himalayan (Li et al., 2022). Consequently, this study integrated the burial history, thermal history, H, TOC, and $R_{eq.}$ distribution map of the Є$_1y$ shale to reconstruct its HG and HE history. The intensity of HG and HE for the five key periods of the source rocks was calculated by Eqs. (8) and (9). The amount of HG and HE for each period was further calculated using Eqs. (11) and (12).

The burial history and thermal history simulation results (Figs. 12 and 13) of key wells (SB 5, MC 1) in different structural units of the TB demonstrate that the Є$_1y$ source rocks generally entered the HGT ($R_{eq.}$ = 0.46%) in the early Ordovician (479 Ma) and began to generate hydrocarbon. This age is consistent with the timing of HG identified by basin modeling (Li et al., 2022) and the

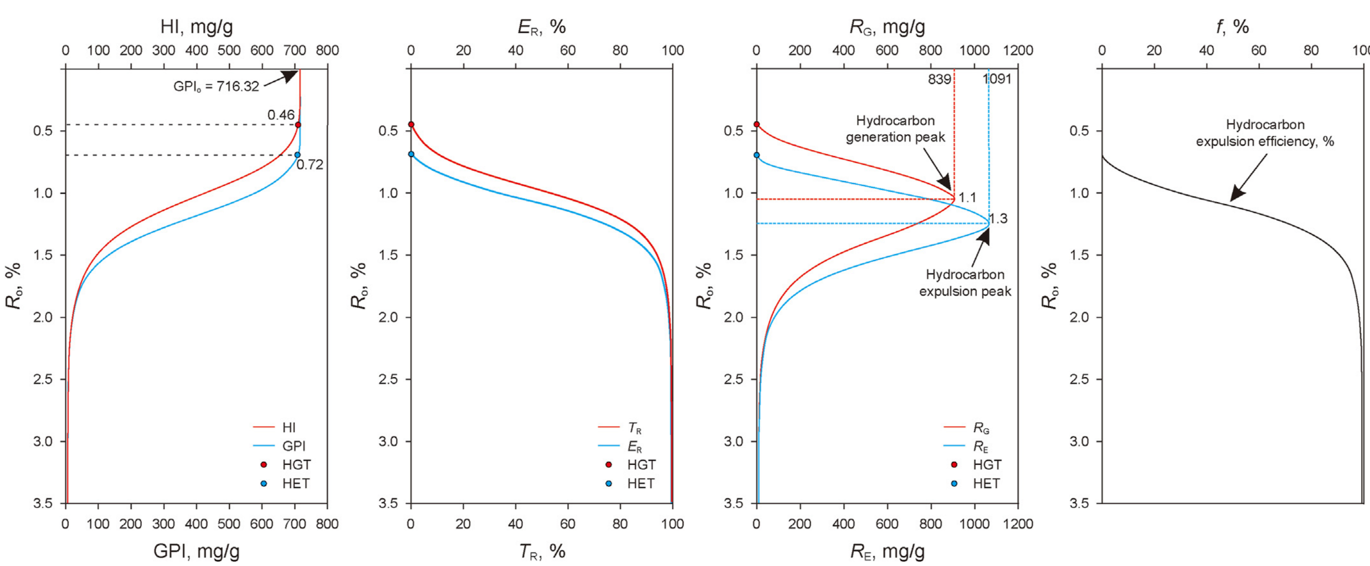

Fig. 11. Comprehensive model for the quantification of HG and HE of the Є$_1y$ shale in the TB (HGT: hydrocarbon generation threshold; HET: hydrocarbon expulsion threshold; E_R: hydrocarbon expulsion ratio; T_R: transformation rate; R_G: hydrocarbon generation rate; R_E: hydrocarbon expulsion rate; f: hydrocarbon expulsion efficiency).

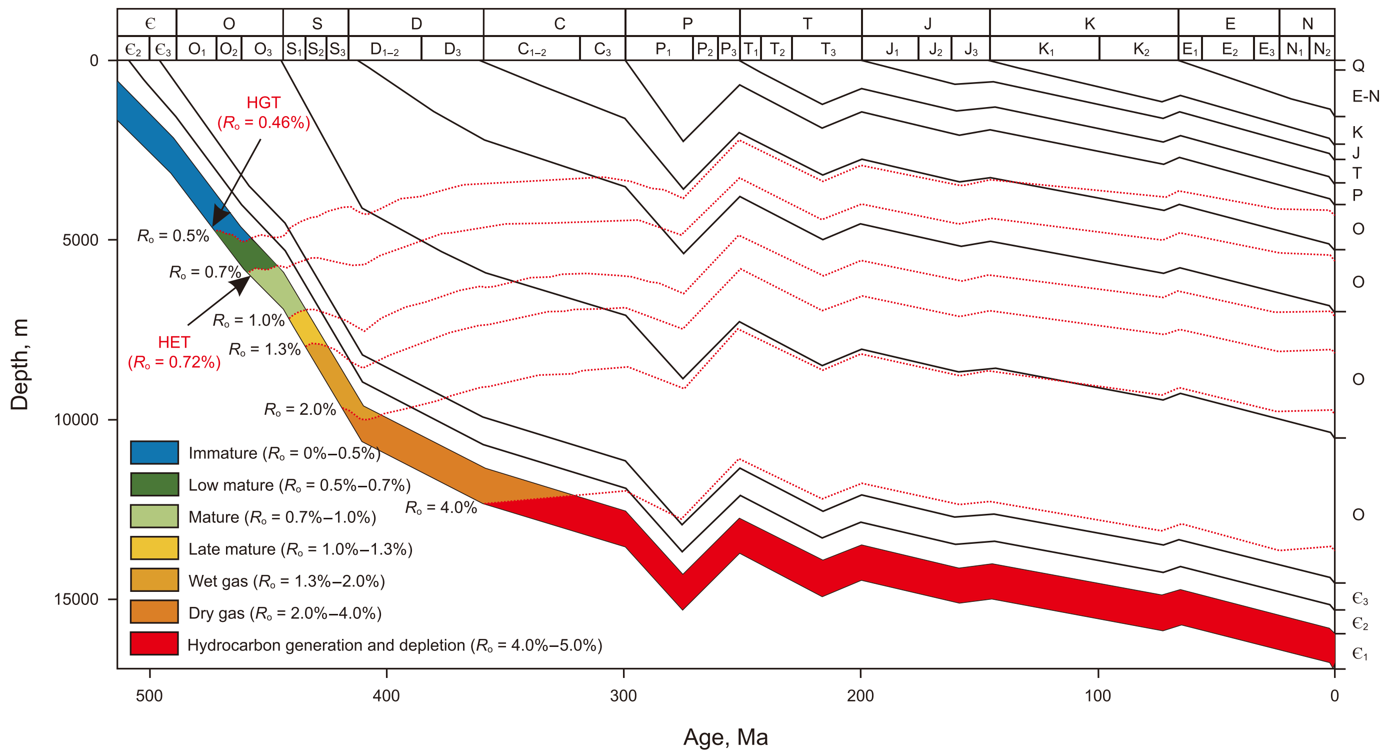

Fig. 12. Thermal evolution and burial history of the $Є_1y$ source rocks, Well MC 1 in the TB (Modified after Zheng et al. (2018)).

Re-Os ages of reservoir oils (Yuan et al., 2024). In the middle Ordovician (452 Ma), the shales reached the HET ($R_{eq.} = 0.72\%$) and began to expel hydrocarbons. During the Ordovician-Silurian period, the rapid sedimentation of the strata and the rapid thermal evolution of the source rocks in the platform area of TB resulted in the overall source rocks entering a mature to high maturity stage, accompanied by a rapid increase in HG. The late Caledonian period (430 Ma) represents the pinnacle of HG, with a multitude of HG processes having been completed (Jia and Zhang, 2023). During this period, three HG centers were located in the midden part of the Manjiaer Depression, the transitional zone of Awati Depression and Manjiaer Depression, and the Tadong area (Fig. S1), with maximum HG intensity of 500×10^4 t/km^2, 600×10^4 t/km^2, and 700×10^4 t/km^2. While other areas in the basin have entered the HGT, the HG intensity is relatively low, generally below 200×10^4 t/km^2. The Southwest Depression, due to its lowest maturity, exhibits a HG intensity that ranges from 0 to 50×10^4 t/km^2. During this period, the intensity of HE was relatively low, with only one HE center in the Manjiaer Depression (Fig. S2), with a maximum HE intensity of 100×10^4 t/km^2. The Awati Depression and Tabei Uplift have not yet entered the HET, while the rest of the area has just begun to enter the HET with an intensity of HE below 50×10^4 t/km^2. The HG center in the early Hercynian is consistent with that in the late Caledonian (Fig. S3), and the HE intensity has increased, with a maximum HE intensity of 450×10^4 t/km^2. Most areas have already entered the HET (Fig. S4). The in-situ calcite U-Pb dating results (420.6–384.6 Ma) provide further confirmation that hydrocarbons generated in the late Caledonian to early Hercynian periods were charged into Cambrian and Ordovician reservoirs (Yuan et al., 2024).

By the late Hercynian, the centers of HG and HE of the $Є_1y$ were consistent with those of the early Hercynian (Fig. S5), with a slight increase in HG intensity. The HG intensity of the three HG centers in the midden part of the Manjiaer Depression, the transitional zone of Awati Depression and Manjiaer Depression, and the Tadong area were 900×10^4 t/km^2, 700×10^4 t/km^2, and 1000×10^4 t/km^2, respectively. Nevertheless, the intensity of HE is considerably higher than that of the early Hercynian (Fig. S6), and the overall source rock of the $Є_1y$ has entered the HET. The HE intensity of the Manjiaer Depression is 700×10^4 t/km^2. While other regions have also entered the HET, the HE intensity remains generally below 100×10^4 t/km^2.

The intensity of HG and HE in the late Yanshan is relatively similar to that in the Late Hercynian However, the range of the HG and HE centers is significantly expanded (Fig. S7). The HG intensity of the two main HG centers in the midden of the Manjiaer Depression, the transitional zone of Awati Depression and Manjiaer Depression reaches 900×10^4 t/km^2 and 1000×10^4 t/km^2, respectively. Nevertheless, the HG intensity in the Southwestern Depression remains below 100×10^4 t/km^2. The HE intensity of the Manjiaer Depression remains unchanged (Fig. S8), but the HE intensity in the transitional zone of the Awati Depression and Manjiaer Depression and the Tadong area has increased, reaching 350×10^4 t/km^2 and 300×10^4 t/km^2, respectively.

By the late Himalayan, the maturity in most areas of the basin had reached over 2.0%, and the thermal evolution was approaching its end. Consequently, the HG and HE characteristics of the $Є_1y$ during this period have remained unchanged to the present day. The current HG intensity is consistent with that of the late Yanshan period (Fig. 14); However, the intensity of HE has exhibited a slight increase from the end of the Jurassic period to the present. The HE intensity of the two HE centers in the eastern part of the Awati Depression and the Keping area is 500×10^4 t/km^2 and 300×10^4 t/km^2, respectively. The HE intensity in the midden part of the Manjiaer Depression remains at 700×10^4 t/km^2, while the HE in the Tadong area has stopped (Fig. 15). In summary, the Manjiaer and Awati areas exhibit greater maturity and OM abundance, as well as thicker source rocks, which collectively serve as the primary

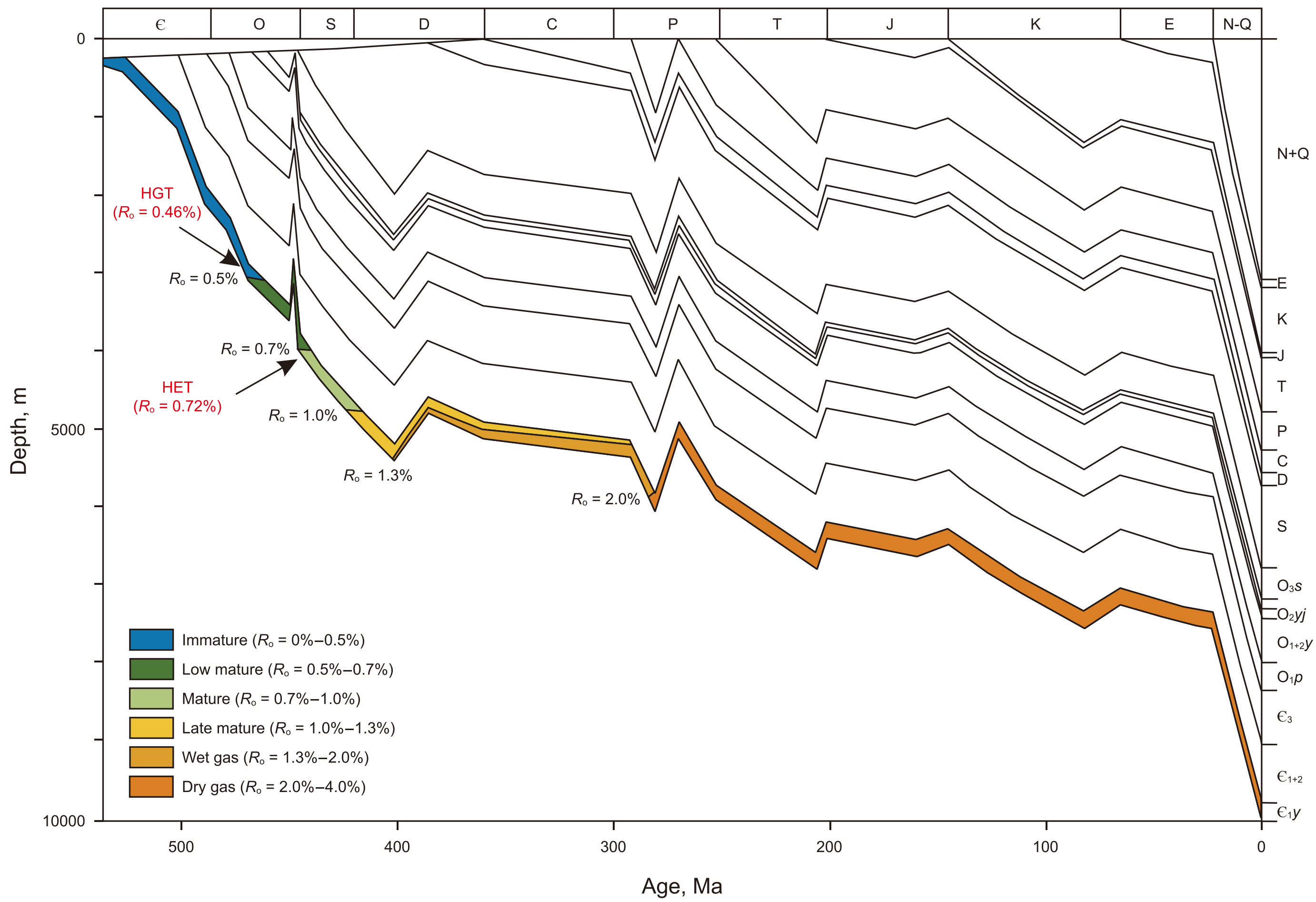

Fig. 13. Thermal evolution and burial history of the $Є_1y$ source rocks, Well SB 5 in the TB (Modified after Yang et al. (2021)).

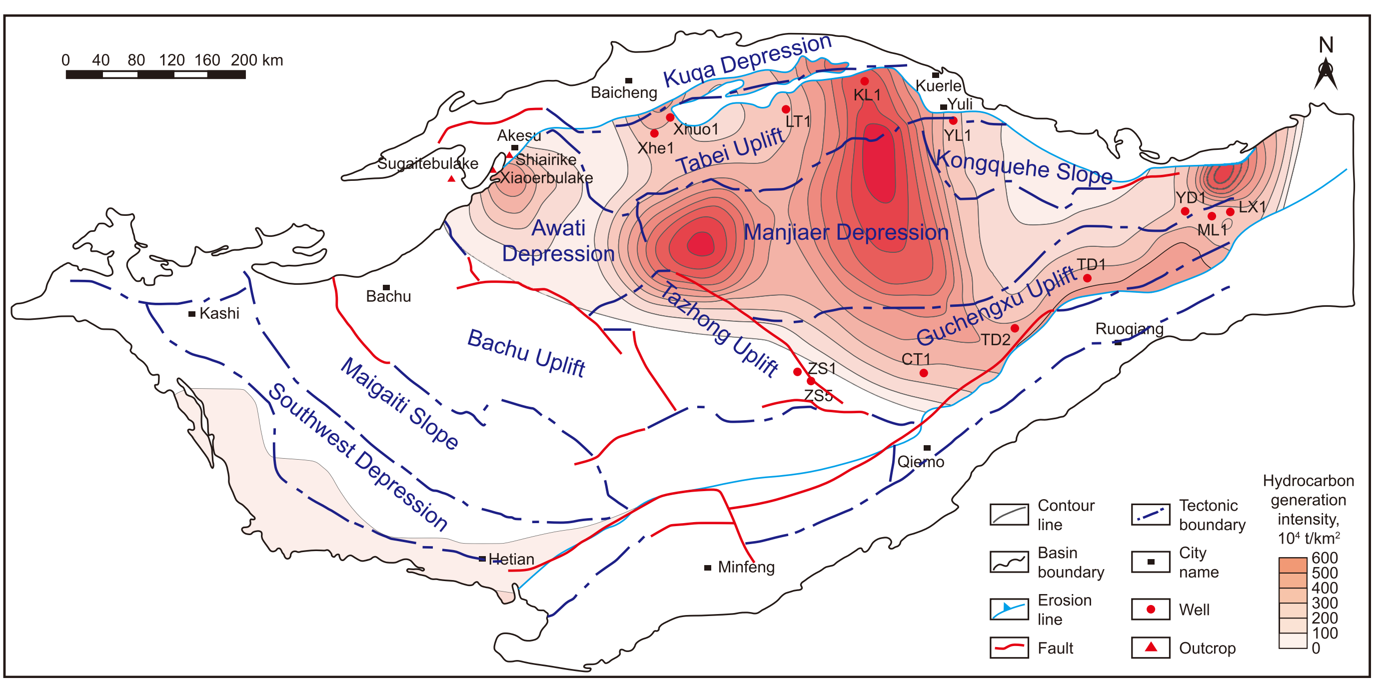

Fig. 14. Current HG intensity of the $Є_1y$ source rocks in the TB.

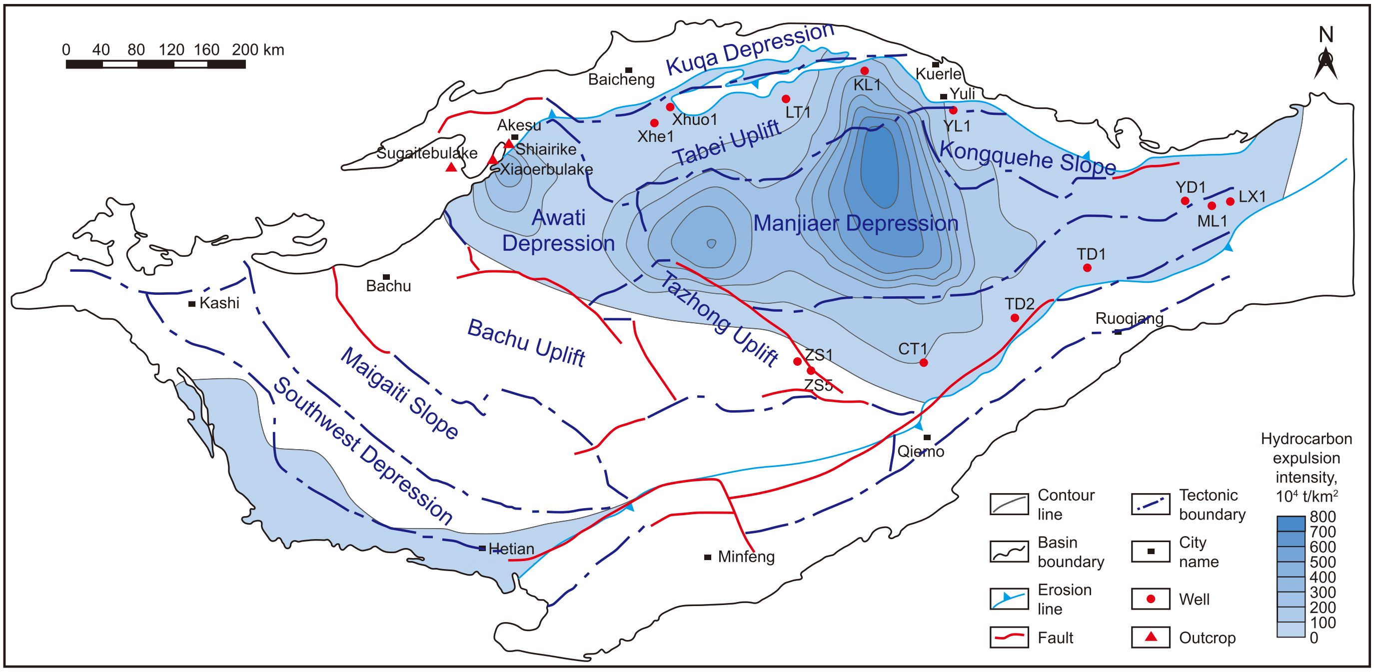

Fig. 15. Current HE intensity of the ϵ_1y source rocks in the TB.

centers of HG and HE throughout geological history.

4.3.3. Hydrocarbon generation and expulsion amounts of ϵ_1y source rocks

The cumulative HG and HE of the ϵ_1y source rocks in different geological periods are illustrated in Fig. 16: the cumulative HG and HE in the late Caledonian were 47.10 $\times$ 10^{10} and 2.66 $\times$ 10^{10} t, respectively; the cumulative HG in the early Hercynian was 54.77 $\times$ 10^{10} t, and the cumulative HE was 10.45 $\times$ 10^{10} t; the cumulative HG and HE in the late Hercynian were 60.77 $\times$ 10^{10} and 21.49 $\times$ 10^{10} t, respectively; the cumulative HG and HE in the late Yanshan were 65.61 $\times$ 10^{10} and 29.92 $\times$ 10^{10} t, respectively; the cumulative HG and HE in the late Xishan were 68.88 $\times$ 10^{10} and 35.59 $\times$ 10^{10} t, respectively. The ϵ_1y source rocks completed a significant number of HG and HE processes in the Late Caledonian and Late Hercynian, accounting for 79.5% of the current cumulative HG and 62% of the current cumulative HE. This provided sufficient oil and gas sources for the formation of the Cambrian and Ordovician hydrocarbon reservoirs in the Paleozoic era of the Hercynian (Yang et al., 2020a; Zhu et al., 2021, 2022).

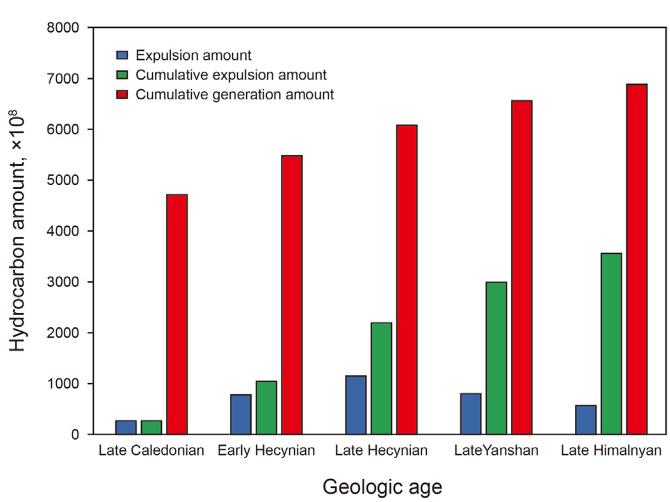

Fig. 16. HG and HE amount of the ϵ_1y source rocks in the TB in geo-history.

5. Discussion

5.1. Evaluation of the resource potential of the ϵ_1y source rocks

The Cambrian-Ordovician hydrocarbon reservoirs are the most significant exploration objective in the TB. Since the discovery of primary hydrocarbon reservoirs in the Middle - Lower Cambrian in the Well ZS 1 in the Tazhong Uplift, the Lower Cambrian source rocks have become one of the key strata for hydrocarbon exploration. The Well LT 1 has obtained high oil flow in the dolomite reservoir of Wusongger Formation (8165–8327 m) of Lower Cambrian, with daily oil production of 134 m^3 and gas production of 45917 m^3 (Yang et al., 2020a, 2020b), which further confirms that the stratum deeper than 8200 m in the TB still has great potential to discover primary oil reservoir and high-quality source-reservoir-cap rock combination. As previously outlined in section 4.3.2, the cumulative HG potential of the ϵ_1y source rocks is estimated to be 68.88 $\times$ 10^{10} t, representing a significant HG capacity. It has been identified by various research methods as the most effective main source rocks for Cambrian-Ordovician deep to ultra-deep hydrocarbon reservoirs in the TB (Zhu et al., 2018), which determines the hydrocarbon potential of the Paleozoic petroleum system in the TB. In this study, the potential hydrocarbon resource potential of the Lower Paleozoic petroleum system in the TB is evaluated by utilizing the HG and HE model of the ϵ_1y source rocks and the resource potential evaluation method.

The research on hydrocarbon sources reveals that a portion of the hydrocarbon generated from the ϵ_1y shale is primarily migrated upward to the Ordovician reservoir through the Cambrian through source fault, influenced by buoyancy. This supports the industrial reserves and production of Ordovician carbonate rock reservoirs in Shunbei, Fuman, and other regions of the TB (Zhu et al., 2019b; Li et al., 2021b). Furthermore, the ϵ_1y source rocks, the reservoir of the Xiaoerbulake Formation (ϵ_1x), and the cap rocks of the Middle Cambrian formed a complete vertical combination of source-reservoir-cap. The hydrocarbons generated by the ϵ_1y were transported to the reservoir of the ϵ_1x platform, where the source rocks were supplied with hydrocarbons in situ and formed reservoirs in situ. The migration and accumulation coefficient represents a pivotal parameter in the genetic evaluation of oil and gas resource potential that varies considerably between various kinds of hydrocarbon reservoirs. This is due to differences in reservoir properties, migration dynamics, migration channels, and preservation conditions (Zheng et al., 2019; Li et al., 2020, 2021a). The statistics of the migration and accumulation coefficients of conventional hydrocarbons in the six major basins of China reveal an average migration and accumulation coefficient for conventional oil at 32.8%, with a migration and accumulation coefficient of 6% for conventional gas, and the average value for both is 19.4% (Pang, 2023). The disparity in distance between the Ordovician reservoir, the ϵ_1x reservoir, and the ϵ_1y source rocks has led to a notable discrepancy in the quantity of oil and gas lost. While the former has experienced a considerable loss, the latter has experienced a relatively minor loss. Consequently, the migration and accumulation coefficients of 9.7% and 19.4% were employed to calculate the resource reserves of the Ordovician reservoir and the ϵ_1x reservoir, respectively. The cumulative HE from the shale of the ϵ_1y is 35.59×10^{10} t. Therefore, the total contribution of the ϵ_1y to the carbonate hydrocarbon reservoir of the Ordovician is 3.45×10^{10} t, while the total resource of the carbonate hydrocarbon reservoir of the ϵ_1x is 6.90×10^{10} t.

The remaining hydrocarbons generated by the ϵ_1y source rocks remain within the interior. The results of the calculations indicate that the residual hydrocarbons in the ϵ_1y are primarily concentrated in the western part of the Manjiaer Depression, the Tabei Uplift, and the Tadong area. The residual hydrocarbon intensity is predominantly situated between 1 and 6×10^6 t/km^2 (Fig. 17). The current cumulative residual hydrocarbon amount is 33.29×10^{10} t, indicating that approximately 50% of the generated hydrocarbons are trapped within the source rocks. The hydrocarbons that occur within the source rocks belong to shale oil and gas, with shorter migration distances and higher migration and accumulation coefficients than conventional hydrocarbons. Accordingly, a 45% migration and accumulation coefficient was employed (Xu et al., 2011; Zheng et al., 2019), which corresponds to a shale oil and gas resource potential of 16.02×10^{10} t. The results indicate promising prospects for deep to ultra-deep hydrocarbon exploration in the TB. Notably, the extensive Cambrian subsalt high-quality dolomite tight reservoirs and the abundant hydrocarbon resources contained within high-quality source rocks demonstrate significant potential. Transitioning from external to internal source rock exploration while continuously approaching hydrocarbon source rocks represents a crucial breakthrough direction for the next step of exploration in the TB.

5.2. Prediction of favorable areas for oil and gas exploration of cambrian subsalt

The formation of hydrocarbon reservoirs is influenced by multiple geological factors. For conventional hydrocarbon reservoirs, source rocks, sedimentary facies, and regional cap rocks play a pivotal role in determining the formation and distribution of hydrocarbons (Pang et al., 2012a). Hydrocarbon source kitchens are the material basis for the formation of hydrocarbon reservoirs, controlling the source of hydrocarbons, and exhibiting the characteristic of "near source accumulation". This means that reservoirs are mainly distributed near the expulsion center of source rocks. The favorable sedimentary facies development area exhibits favorable reservoir physical properties, controlling the distribution range of hydrocarbons, exhibiting the characteristic of "favorable facies controlling reservoirs". The continuous and stable distribution of effective regional cap rocks can protect reservoirs effectively, controlling their planar distribution. Research has shown that the algae limestone flat, internal shoal, and platform margin reef - beach are optimal reservoirs for the ϵ_1x (Jiang et al., 2021). The algae limestone flat and internal shoal are mainly distributed

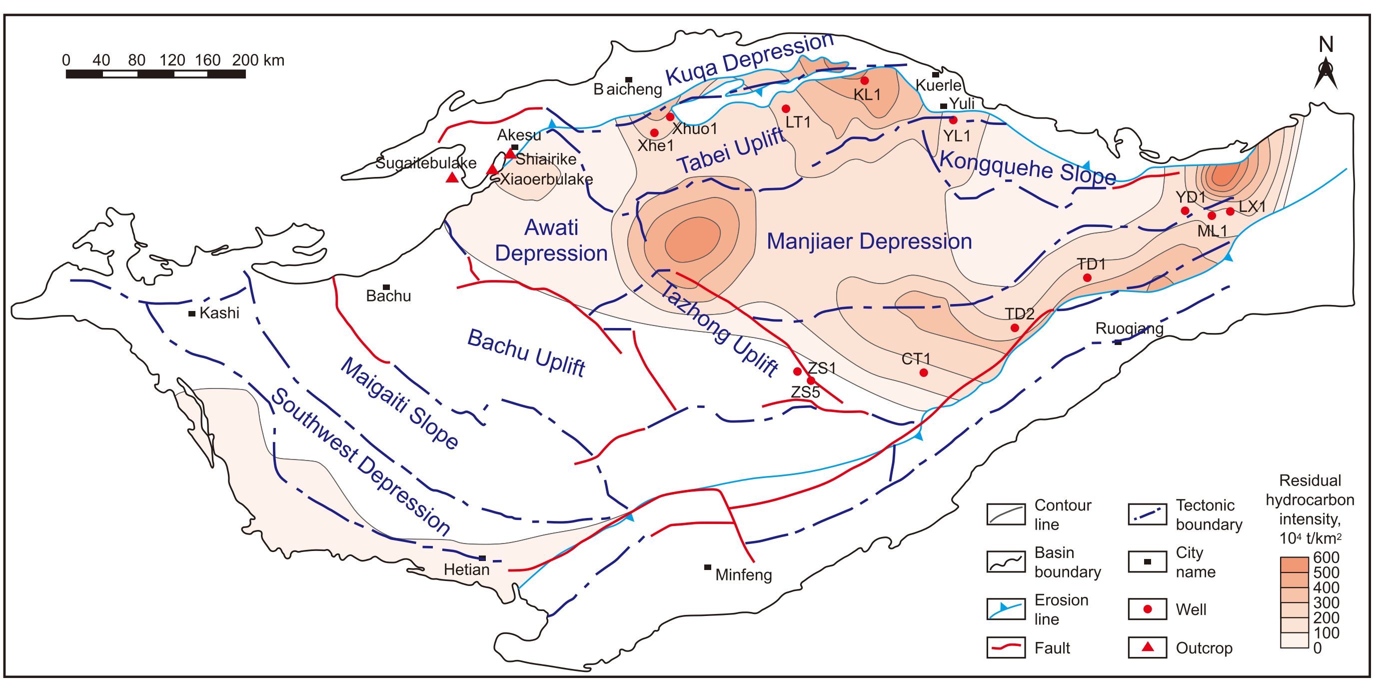

Fig. 17. Current residual hydrocarbon intensity of the ϵ_1y source rocks in the TB.

around the paleo-uplift, and are extensively developed in the Bachu Uplift, Tazhong Uplift, Lunnan Low Uplift, Manxi Low Uplift, with a porosity of 1.9%–9.6% and a reservoir thickness of 20–70 m; The platform margin reef-beach is continuously dispersed in the northern part of the Tabei Uplift and Lunnan-Gucheng area, with porosity ranging from 2.0% to 5.6% (Yi et al., 2019). The Bachu Uplift, Awati Depression, Tazhong Uplift, and Tabei Uplift as well as the western Manxi Low Uplift have developed large areas of gypsum salt rock layers with a thickness of 200–450 m, providing good cap rock conditions for hydrocarbon accumulation in the ϵ_1x (Du and Pan, 2016). At present, the Cambrian undersalt hydrocarbon reservoirs that have been discovered are primarily distributed in the reservoirs of the algae limestone flat, internal shoal, and platform margin reef-beach, and all are distributed under high-quality gypsum salt rock cap rocks, and located near the HE center of the $\epsilon_1 y$, significant control of hydrocarbon formation by source rocks, sedimentary facies and cap rocks. Based on the HG and HE characteristics of the $\epsilon_1 y$, in combination with the distribution of the sedimentary facies of the Cambrian ϵ_1x reservoir (Yi et al., 2019) and the distribution of the Middle Cambrian gypsum-salt cap rocks (Du and Pan, 2016), the favorable exploration areas for hydrocarbons of the Cambrian subsalt of the TB were predicted, and three types of exploration favorable areas were divided (Fig. 18; Table 1). Among them, Class I favorable areas have a complete assemblage of source-reservoir-cap, and their conditions for reservoir formation and preservation are the most favorable; Class II favorable areas lack any favorable conditions among source stoves, favorable reservoirs, and high-quality cap rocks, followed by their reservoir formation and preservation conditions; and Class III favorable areas have only a single reservoir formation condition, with the lowest probability of forming large-scale hydrocarbon reservoirs. In addition to the industrial oil and gas drilling areas that have been discovered, the Awati Depression and the western region of Manxi have high hydrocarbon expulsion intensity, which can provide sufficient oil and gas resources. High-quality reservoirs such as the algae limestone flat, internal shoal, and platform margin reef-beach are also developed, and the thickness of gypsum salt rock cap rock is relatively thick, which is conducive to accumulating and preserving hydrocarbons and it can be regarded as favorable areas for further exploration and development.

5.3. Implications

This paper calculated the hydrocarbon expulsion of the $\epsilon_1 y$ source rocks in the Tarim Basin during key periods. The current cumulative hydrocarbon expulsion reaches 35.59×10^{10} t, which provides important evidence for the $\epsilon_1 y$ as the main source rock for hydrocarbon supply and filling the gap in hydrocarbon expulsion calculation in the study area and is of some significance in guiding the deployment of the next step of hydrocarbon exploration. It should be pointed out that during the maturation of organic matter, the loss of light hydrocarbons in S_1 will affect the calculation results of hydrocarbon generation and hydrocarbon expulsion. Since some of the data collected in this study did not list the S_1 value, the lack of light hydrocarbon recovery may result in the calculation of hydrocarbon generation and hydrocarbon expulsion to be smaller than the actual value. In addition, the accuracy of hydrocarbon generation/expulsion assessment and resource potential evaluation depends on three core elements: (1) Completeness of fundamental geological data (well logging, seismic data, core analysis); (2) Reliability of source rock thickness maps, TOC distribution maps, and maturity maps; (3) Scientific basis for selecting migration-accumulation coefficients. Existing geological maps primarily rely on historical well logging and seismic interpretation results, providing critical constraints for source rock evaluation in data-limited areas. However, their precision is inherently constrained by the quality of original data and interpretation methodology systems. The continuous advancement of exploration/development technologies and progressive accumulation of actual geological data will enable more precise determination of source rock quality and hydrocarbon generation potential. This will allow calculated resource estimates to gradually approach actual oil and gas resource volumes. In the future, we will integrate more measured data and further refine the hydrocarbon generation and expulsion

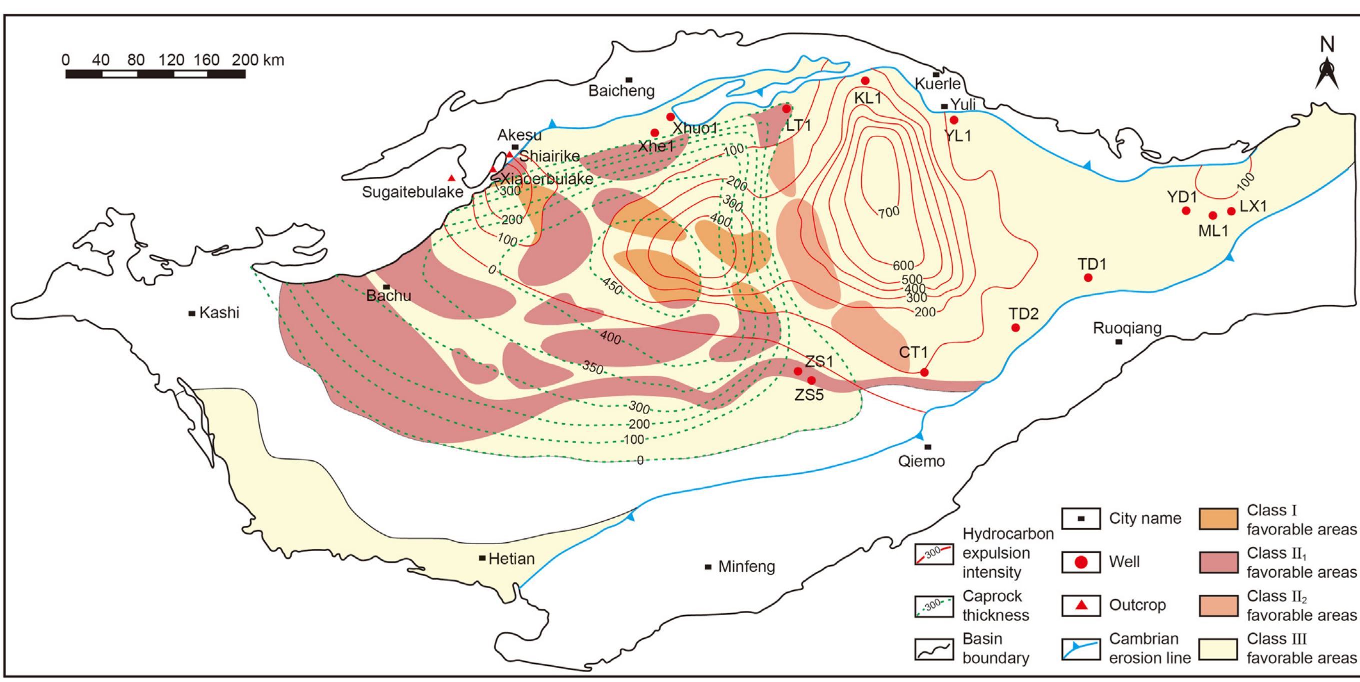

Fig. 18. Favorable areas for oil and gas exploration of Cambrian subsalt in the TB.

Table 1
Classification and evaluation criteria for favorable areas.

Classification standard	Hydrocarbon expulsion intensity, 10^4 t/km^2	Favorable reservoirs (algae limestone flat, internal shoal, and platform margin reef-beach)	Gypsum-salt caprock
Class I favorable areas	>100	√	√
Class II$_1$ favorable areas	×	√	√
Class II$_2$ favorable areas	>100	√	×
Class III favorable areas	√	×	×
	×	√	×
	×	×	√

Note: "√" indicates the presence of favorable conditions for hydrocarbon accumulation, and " × " indicates the absence.

models based on the distinct geological characteristics of the eastern and western regions, thereby significantly enhancing the accuracy of oil and gas resource assessments and providing a more reliable foundation for the exploration and development of hydrocarbon resources. Finally, the distribution law of hydrocarbon in the Tarim Basin is very complex. The oil and gas reservoirs have undergone a complex process of multiple charging and multi-stage adjustment. During the migration process, oil and gas are also affected by a series of complex factors, such as fault development, fluid activity, phase transformation, and so on (Cai et al., 2001; Zhang et al., 2018; Zhu et al., 2018). The expelled hydrocarbons have not completely migrated to favorable traps, and after accumulation, they generally undergo secondary geochemical alterations such as biodegradation, gas invasion fractionation, thermochemical sulfate reduction (TSR), and thermal cracking. For example, the Ordovician reservoirs in the northern Halahatang and the western low-uplift areas of Lunnan have experienced varying degrees of biodegradation due to poor sealing conditions and active microbial activities (Zhang et al., 2014). The high development of fault systems and unconformities in the eastern regions of Tazhong and the northern Tabei areas has led to the complex distribution of hydrocarbon phase states due to differential gas invasion alteration (Yang and Zhu, 2013). In the Gucheng-Shunnan area, the Ordovician gas reservoirs have shown the presence of significant amounts of dry bitumen due to thermal cracking (Zhou et al., 2019). Some wells in the Tazhong area, heavily altered by TSR, have oils rich in medium to high concentrations of sulfur-containing compounds such as thiadiamondoids and high concentrations of H_2S (Zhu et al., 2019a; Jia et al., 2020). The H_2S concentration produced during TSR is five times the current reservoir H_2S concentration (Hutcheon et al., 1995), potentially causing late-stage non-selective dissolution (Moore and Druckman, 1981). The dolomite reservoirs in the upper section of the Cambrian Xiaoerbulake Formation, interlayered with evaporites, can increase porosity by approximately 3% under TSR conditions. Recent studies have simulated that TSR can convert at least 38.9% of liquid hydrocarbons into pyrobitumen (Sun et al., 2024). Therefore, it is evident that hydrocarbons in different regions of the Tarim Basin have undergone various types and degrees of secondary geochemical alterations after accumulation, significantly impacting the assessment of hydrocarbon resource types and potential. Consequently, it is necessary to highlight that our current evaluation results represent the theoretical maximum recoverable resources, and future detailed assessments and in-depth research on resource potential in different areas, considering the actual geological alterations, are imperative.

6. Conclusion

In this study, the hydrocarbon generation and hydrocarbon expulsion potential of high-quality source rocks of the Lower Cambrian high-maturity to over-maturity Є$_1y$ in the Tarim Basin were evaluated by using the hydrocarbon generation potential method based on the latest ultra-deep well drilling data and data-driven Monte Carlo simulation techniques, and the potential hydrocarbon resources of the Lower Paleozoic petroleum system were determined quickly and effectively based on the genetic method. Furthermore, three favorable areas were predicted. The high-quality source rocks of the Є$_1y$ enter the hydrocarbon generation threshold and expulsion threshold at equivalent vitrinite reflectances of 0.46% ($R_{eq.}$) and 0.72% ($R_{eq.}$), respectively, and reach the hydrocarbon generation peak and expulsion peak at $R_{eq.}$ values of 1.1% and 1.3%, respectively., with an average expulsion efficiency of 73%. The cumulative hydrocarbon generation is 68.88×10^{10} t, the cumulative expulsion amount is 35.59×10^{10} t, and the residual hydrocarbon amount is 33.29×10^{10} t. The Awati Depression and the Manjiaer Depression have always been the centers of hydrocarbon generation and expulsion for the Є$_1y$ source rocks. The Cambrian reservoirs in the Tarim Basin possess enormous oil and gas potential, with the total resource amount of conventional carbonate oil and gas reservoirs in the Є$_1$x being 6.90×10^{10} t, and the shale oil and gas resources within the Yuertusi Formation amounting to 16.02×10^{10} t. The transition zone between the Awati Depression and the Manjiaer Depression is mainly classified as Class I favorable areas, which has higher hydrocarbon expulsion intensity and is closer to the hydrocarbon expulsion center. High-quality reservoirs such as the algae limestone flat, internal shoal, and platform margin reef-beach are developed, and the thickness of gypsum salt rock cap rocks is relatively thick, which is conducive to the accumulation and preservation of oil and gas. It can be used as a favorable area for further exploration and development.

CRediT authorship contribution statement

Yao Hu: Writing – original draft, Investigation, Conceptualization. **Cheng-Zao Jia:** Writing – review & editing, Supervision. **Jun-Qing Chen:** Writing – review & editing, Investigation. **Xiong-Qi Pang:** Writing – review & editing, Supervision. **Chen-Xi Wang:** Validation, Software. **Hui-Yi Xiao:** Investigation. **Cai-Jun Li:** Investigation. **Yu-Jie Jin:** Investigation.

Declaration of competing interest

The authors declare that they have no known competing financial interests or personal relationships that could have appeared to influence the work reported in this paper.

Acknowledgments

This research is supported by the CNPC Science and Technology Major Project of the Fourteenth Five-Year Plan (2021DJ0101) and the National Natural Science Foundation of China (U19B6003-02,41872148). We highly appreciate the leaders and experts of the Tarim Oilfield Company, PetroChina, as well as the scientists from our research group. We also appreciate the professional suggestions and comments from the editor and anonymous reviewers.

Nomenclature

Definitions and explanations of the relevant abbreviation and terms

$Є_1y$	Yuertusi Formation
$Є_1x$	Xiaoerbulake Formation
TB	Tarim Basin
TOC	Total organic carbon (in wt.%)
R_{eq}	Equivalent vitrinite reflectance
OM	Organic matter
HCI	Hydrocarbon index, defined as free hydrocarbons (S_1) divided by TOC×100 (in mg HC/g TOC)
HI	Hydrogen index, defined as pyrolysis hydrocarbon (S_2) divided by TOC×100 (in mg HC/g TOC
GPI	Hydrocarbon generation potential index, defined as the sum of the free hydrocarbons (S_1) and the pyrolysis hydrocarbon (S_2) divided by TOC×100 (in mg HC/g TOC)
HI_o	Original hydrogen index
GPI_o	Original hydrocarbon generation potential index
HGPM	Hydrocarbon generation potential method
HG	Hydrocarbon generation
HE	Hydrocarbon expulsion
HGT	Hydrocarbon generation threshold
HET	Hydrocarbon expulsion threshold
R_G	Hydrocarbon generation rate
R_E	Hydrocarbon expulsion rate
E_R	Expulsion ratio calculated from GPI_o and GPI
T_R	Transformation ratio calculated from HI_o, HI, and HCI
f	Hydrocarbon expulsion efficiency, the expelled hydrocarbon divided by total hydrocarbon generated
α	Represent each gram of organic carbon lost that can generate α grams of hydrocarbon

Appendix A. Supplementary data

Supplementary data to this article can be found online at https://doi.org/10.1016/j.petsci.2024.12.001.

References

Burton, Z.F.M., Moldowan, J.M., Sykes, R., et al., 2018. Unravelin petroleum degradation, maturity, and mixing and addressing impact on petroleum prospectivity: insights from frontier exploration regions in New Zealand. Energy Fuels 32, 1287–1296. https://doi.org/10.1021/acs.energyfuels.7b03261.

Cai, C.F., Hu, W.S., Worden, R.H., 2001. Thermochemical sulphate reduction in cambro-ordovician carbonates in central tarim. Mar. Petrol. Geol. 18 (6), 729–741. https://doi.org/10.1016/S0264-8172(01)00028-9.

Campbell, I.H., Allen, C.M., 2008. Formation of supercontinents linked to in creases in atmospheric oxygen. Nat. Geosci. 1 (8), 554–558. https://doi.org/10.1038/ngeo259.

Canfield, D.E., Poulton, S.W., Narbonne, G.M., 2007. Late-Neoproterozoic deep-ocean oxygenation and the rise of animal life. Science 315 (5808), 92–95. https://doi.org/10.1126/science.1135013.

Chen, Q.L., Chu, C.L., Hu, G., et al., 2017. Sedimentary characteristics and depositional environment of Yuertusi Formation in keping area, Tarim Basin. Petroleum Geology & Experiment 39 (3), 311–317+326. https://doi.org/10.11781/sysydz201703311 (in Chinese).

Chen, W.Y., Zhu, G.Y., Zhang, K.J., et al., 2020. Late Neoproterozoic intracontinental rifting of the Tarim carton, NW China: an integrated geochemical, geochronological and Sr-Nd-Hf isotopic study of siliciclastic rocks and basalts from deep drilling cores. Gondwana Res. 80, 142–156. https://doi.org/10.1016/j.gr.2019.10.007.

Chen, Z.H., Jiang, C.Q., Denis, L., et al., 2016. Model-assisted Rock-Eval data interpretation for source rock evaluation: examples from producing and potential shale gas resource plays. Int. J. Coal Geol. 165 (1), 290–302. https://doi.org/10.1016/j.coal.2016.08.026.

Craig, J., Biffi, U., Galimberti, R.F., et al., 2013. The palaeobiology and geochemistry of Precambrian hydrocarbon source rocks. Mar. Petrol. Geol. 40, 1–47. https://doi.org/10.1016/j.marpetgeo.2012.09.011.

Deng, Q., 2021. Sedimentary Geochemical Records and Organic Matter Accumulation Mechanisms in the Sinian-Lower Cambrian Strata: Case Studies in South China and the Tarim Basin, NW China. Guangzhou Institute of Geochemistry. Chinese Academy of Sciences. https://doi.org/10.1016/j.jseaes.2020.104660.

Deng, Q., Wang, H.Z., Wei, Z.W., et al., 2021. Different accumulation mechanisms of organic matter in Cambrian sedimentary successions in the western and northeastern margins of the Tarim Basin, NW China. J. Asian Earth Sci. 207, 104660. https://doi.org/10.1016/j.jseaes.2020.104660.

Du, J., Pan, W., 2016. Accumulation conditions and play targets of oil and gas in the Cambrian subsalt dolomite, Tarim Basin, NW China. Petrol. Explor. Dev. 43 (3), 327–339. https://doi.org/10.1016/S1876-3804(16)30043-X (in Chinese).

Eigenbrode, J.L., Freeman, K.H., 2006. Late Archean rise of aerobic microbial ecosystems. P. Natl. Acad. Sci. USA. 103 (43), 15759–15764. https://doi.org/10.1073/pnas.0607540103.

Erwin, D.H., Laflamme, M., Tweedt, S.M., et al., 2011. The Cambrian conundrum: early divergence and later ecological success in the early history of animals. Science 334 (6059), 1091–1097. https://doi.org/10.1126/science.1206375.

Fan, Q., Fan, T., Li, Y., et al., 2020. Paleo-Environments and development Pattern of high-quality marine source rocks of the early Cambrian, Northern Tarim platform. Earth Sci. 45 (1), 285–302. https://doi.org/10.3799/dqkx.2018.128 (in Chinese).

Feng, G.X., Chen, S.J., 1988. Relationship between the natural reflectance of bitumen and vitrinite in rock. Gas Ind. 8 (3), 20–25 (in Chinese).

Gao, Z.Q., Shi, J.Y., Lv, J.L., et al., 2022. High-frequency sequences, geochemical characteristics, formations, and distribution predictions of the lower Cambrian Yuertusi Formation in the Tarim Basin. Mar. Petrol. Geol. 146, 105966. https://doi.org/10.1016/j.marpetgeo.2022.105966.

Ge, Y.W., Li, K., 2014. On geochemical characteristics of sourcerock of the lower cambrian yuertusi formation in Tarim Basin. J. Chongqing Univ. Sci. Tech. 16 (1), 8–12. https://doi.org/10.19406/j.cnki.cqkjxyxbzkb.2014.01.003 (Natural Sciences Edition) (in Chinese).

Grosjean, E., Love, G.D., Stalvies, C., et al., 2009. Origin of petroleum in the neoproterozoic-cambrian south Oman salt basin. Org. Geochem. 40 (1), 87–110. https://doi.org/10.1016/j.orggeochem.2008.09.011.

Guo, Q.J., Strauss, H., Zhu, M.Y., et al., 2011. High resolution organic carbon isotope stratigraphy from a slope to basinal setting on the Yangtze Platform, South China: implications for the Ediacaran-Cambrian transition. Precambrian Res. 255, 209–217. https://doi.org/10.1016/j.precamres.2011.10.003.

Han, H.Y., 2017. The Sedimentary Model and Hydrocarbon Generation Potential of Yurtus Formation Source Rocks in Tarim Basin. PHD thesis (in Chinese),. China University of Geosciences, (Beijing).

Handson, A.D., Zhang, S.C., Moldowan, J.M., et al., 2000. Molecular organic geochemistry of the Tarim Basin, northwest China. AAPG Bull. 84 (8), 1109–1128. https://doi.org/10.1306/A9673C52-1738-11D7-8645000102C1865D.

Hartkopf, F.C., Konigshof, P., Littke, R., et al., 2015. Optical thermal maturity parameters and organic geochemical alteration at low grade diagenesis to anchimetamorphism: a review. Int. J. Coal Geol. 150, 74–119. https://doi.org/10.1016/j.coal.2015.06.005.

He, D.F., Jia, C.Z., Li, D.S., 2005. Formation and evolution of polycyclic superimposed Tarim Basin. Oil Gas Geol. 26 (1), 64–77 (in Chinese).

He, T.H., Li, W.H., Lu, S.F., et al., 2022. Mechanism and geological significance of anomalous negative $\delta 13C_{kerogen}$ in the lower cambrian, NW Tarim Basin, China. J. Petrol. Sci. Eng. 208, 109384. https://doi.org/10.1016/j.petrol.2021.109384.

He, T.H., Lu, S.F., Li, W.H., et al., 2020a. Paleoweathering, hydrothermal activity and organic matter enrichment during the formation of earliest Cambrian black strata in the northwest Tarim Basin, China. J. Petrol. Sci. Eng. 189, 106987. https://doi.org/10.1016/j.petrol.2020.106987.

He, T.H., Lu, S.F., Li, W.H., et al., 2020b. Geochemical characteristics and effectiveness of thick, black shales in southwestern depression. Tarim Basin. J. Petrol. Sci. Eng. 185, 106607. https://doi.org/10.1016/j.petrol.2019.106607.

Hu, G., Meng, Q.Q., Wang, J., et al., 2018. The original organism assemblages and kerogen carbon isotopic compositions of the early Paleozoic source rocks in the Tarim Basin, China. Acta. Geol. Sin-Engl. 92 (6), 2297–2309. https://doi.org/10.1111/1755-6724.13729.

Hu, Z.Q., Gao, Z.Q., Liu, Z.B., et al., 2022. Characteristics of Cambrian tectonic-lithofacies paleogeography in China and the controls on hydrocarbons. J. Petrol. Sci. Eng. 214, 110473. https://doi.org/10.1016/j.petrol.2022.110473.

Hui, S.S., Pang, X.Q., Jiang, F.J., et al., 2024. Quantitative effect of kerogen type on the hydrocarbon generation potential of Paleogene lacustrine source rocks, Liaohe Western Depression, China. Petrol. Sci. 21 (1), 14–30. https://doi.org/10.1016/j.petsci.2023.09.004.

Hunt, J.M., 1995. Petroleum Geochemistry and Geology (Textbook). Petrol. Geochem. Geol., 2nd Ed. WH Freeman Company.

Hutcheon, I., Krouse, H.R., Abercrombie, H.J., 1995. Controls on the origin and distribution of elemental sulfur, H_2S, and CO_2 in Paleozoic hydrocarbon reservoirs in western Canada. Geochemical transformations of sedimentary sulfur. ACS (Am. Chem. Soc.) Symp. Ser. 612, 426–438. https://doi.org/10.1021/BK-1995-0612.CH024.

Jia, C.Z., Zhang, S.C., 2023. The formation of marine ultra-deep petroleum in China. Acta Geol. Sin. 97 (9), 2775–2801. https://doi.org/10.19762/j.cnki.dizhixuebao.2023201 (in Chinese).

Jia, L.Q., Cai, C.F., Zhang, J.G., et al., 2020. Effect of thermochemical sulfate reduction on carbonate reservoir quality: cambrian and Ordovician oilfield, Tazhong area, Tarim basin. China. Mar. Petrol. Geol. 123, 104745. https://doi.org/10.1016/

j.marpetgeo.2020.104745.
Jiang, H., Pang, X.Q., Shi, H.S., et al., 2015. Source rock characteristics and hydrocarbon expulsion potential of the Middle Eocene Wenchang formation in the Huizhou depression, Pearl River Mouth basin, south China sea. Mar. Petrol. Geol. 67, 635–652. https://doi.org/10.1016/j.marpetgeo.2015.06.010.
Jiang, W.M., Luo, Q.Q., Shi, K.B., et al., 2021. Origin of a microbial-dominated carbonate reservoir in the lower cambrian xiaoerbulake formation, bachu-tazhong area, tarim basin, NW China. Mar. Petrol. Geol. 113, 105254. https://doi.org/10.1016/j.marpetgeo.2021.105254.
Katz, B.J., 1983. Limitations of 'Rock-Eval' pyrolysis for typing organic matter. Org. Geochem. 4 (3), 195–199. https://doi.org/10.1016/0146-6380(83)90041-4.
Katz, B.J., 2001. Geological Challenges of Exploration, Onshore China, with Special Focus on the Tarim and Junggar Basins, 74. AAPG Memoir, pp. 319–334.
Li, B., Zhang, X., Guo, Q., et al., 2022. Basin modeling of cambrian ultra-deep petroleum system in tarim Basin. Acta petrol. Sin. 43 (6), 804–815. https://doi.org/10.7623/syxb202206005 (in Chinese).
Li, C.R., Pang, X.Q., Huo, Z.P., et al., 2020. A revised method for reconstructing the hydrocarbon generation and expulsion history and evaluating the hydrocarbon resource potential: example from the first member of the Qingshankou Formation in the Northern Songliao Basin, Northeast China. Mar. Petrol. Geol. 121, 104577. https://doi.org/10.1016/j.marpetgeo.2020.104577.
Li, C.R., Pang, X.Q., Ma, X.H., et al., 2021a. Hydrocarbon generation and expulsion characteristics of the Lower Cambrian Qiongzhusi shale in the Sichuan Basin, Central China: implications for conventional and unconventional natural gas resource potential. J. Pet. Sci. Eng. 204, 108610. https://doi.org/10.1016/j.petrol.2021.108610.
Li, F., Zhu, G.Y., Lv, X.X., 2021b. The disputes on the source of Paleozoic marine oil and gas and the determination of the Cambrian system as the main source rocks in Tarim Basin. Acta Petrol. Sin. 42 (11), 1417–1436. https://doi.org/10.7623/syxb202111002 (in Chinese).
Li, M., Pang, X.Q., Luo, B., et al., 2021c. Application of hydrocarbon generation potential method to deep shale gas resource evaluation: a case study of high-quality source rocks of the Wufeng-Longmaxi formation in the Sichuan Basin. J. China Univ. Min. Technol. 50 (6), 1096–1107. https://doi.org/10.13247/j.cnki.jcumt.001301 (in Chinese).
Li, S.M., Pang, X.Q., Yang, H.J., et al., 2010. Generation, migration and accumulation model for the marine oils in the Tarim Basin. Earth Sci. 35 (4), 663–673. https://doi.org/10.3799/dqkx.2010.081 (in Chinese).
Li, T.T., Zhang, Y.J., Zhu, G.Y., et al., 2023. Environmental controls on organic matter enrichment of the lower Cambrian source rocks in the Tarim Basin, Northwest China. Mar. Petrol. Geol. 158, 106539. https://doi.org/10.1016/j.marpetgeo.2023.106539.
Liu, C.G., Qi, L.X., Liu, Y.L., et al., 2016a. Positive carbon isotope excursions: global correlation and genesis in the Middle-Upper Ordovician in the northern Tarim Basin, Northwest China. Petrol. Sci. 13 (2), 192–203. https://doi.org/10.1007/s12182-016-0096-3.
Liu, H., 2015. Discussion on the origin of the reversal stable carbon isotope distributions between kerogen and its derivatives, and the geochemical significances to the marine crude oil reservoirs in Tarim Basin, NW China. PHD thesis,. Guangzhou Institute of Geochemistry, Chinese Academy of Sciences (in Chinese).
Liu, W., Gao, P., Xiao, X.M., et al., 2024. Variable depositional environments and organic matter enrichment of Early Cambrian shales in the Middle Yangtze region, South China. J. Asian Earth Sci. 259, 105874. https://doi.org/10.1016/j.jseaes.2023.105874.
Liu, W.H., Hu, G., Tenger, et al., 2016b. Organism assemblages in the Paleozoic source rocks and their implications. Oil Gas Geol. 37 (5), 617–626. https://doi.org/10.11743/ogg20160501 (in Chinese).
Liu, Z.F., Xiao, X.M., Fu, J.M., et al., 1999. Marine vitrnite reflectance as a maturity indicator of Lower Paleozoic hydrocarbon source rocks. Geochimica 28 (6), 580–588.
Lyons, T.W., Reinhard, C.T., Planavsky, N.J., 2014. The rise of oxygen in Earth's early ocean and atmosphere. Nature 506 (7488), 307–315. https://doi.org/10.1038/nature13068.
Moore, C.H., Druckman, Y., 1981. Burial diagenesis and porosity evolution, upper jurassic smackover, Arkansas and Louisiana. AAPG Bull. 65 (4), 597–628. https://doi.org/10.1306/2F919995-16CE-11D7-8645000102C1865D.
Och, L.M., Shields, Z., Graham, A., 2012. The Neoproterozoic oxygenation event: environmental perturbations and biogeochemical cycling. Earth Sci. Rev. 110 (1–4), 26–57. https://doi.org/10.1016/j.earscirev.2011.09.004.
Pang, X.Q., Zhou, X.Y., Jiang, Z.X., et al., 2012a. Hydrocarbon reservoirs formation, evolution, prediction and evaluation in the Superimposed Basins. Acta Geol. Sin. 86 (1), 1–103 (in Chinese). doi:11-1951/p.20120104.1640.009.
Pang, X.Q., 2023. Evaluation of the global oil and gas resources. In: Quantitative Evaluation of Whole Petroleum System-Hydrocarbon Thresholds and Their Application. Springer Nature Singapore, Singapore, pp. 369–406.
Pang, X.Q., Li, M.W., Li, S.M., et al., 2005. Geochemistry of petroleum systems in the Niuzhuang south slope of Bohai Bay Basin: Part 3. Estimating petroleum expulsion from the Shahejie formation. Org. Geochem. 36, 497–510. https://doi.org/10.1016/j.orggeochem.2004.12.001.
Pang, X.Q., Yu, Q.H., Guan, X.Y., et al., 2012b. Evolution and movement of source kitchens and their control of oil and gas in the Tarim Cratonic Basin. Energy Explor. Exploit. 30 (2), 239–272. https://doi.org/10.1260/0144-5987.30.2.239.
Parfenova, T.M., Kontorovich, A.E., Borisova, L.S., et al., 2010. Kerogen from the cambrian deposits of the kuonamka formation (northeastern siberian platform). Russ. Geol. Geophys. 51 (3), 277–285. https://doi.org/10.1016/j.rgg.2010.02.004.
Peters, K.E., 1986. Guidelines for evaluating petroleum source rock using programmed pyrolysis. AAPG Bull. 70, 318–329. https://doi.org/10.1306/94885688-1704-11D7-8645000102C1865D.
Peters, K.E., Burnham, A.K., Walters, C.C., 2015. Petroleum generation kinetics: single versus multiple heating-ramp open-system pyrolysis. AAPG Bull. 99 (4), 591–616. https://doi.org/10.1306/11141414080.
Peters, K.E., Cassa, M.R., 1994. Applied Source-Rock Geochemistry, 60. AAPG Memoir, pp. 93–120.
Peters, K.E., Walters, C.C., Moldowan, J.M., 2005. Biomarkers and Isotopes in the Petroleum Exploration and Earth History: the Biomarker Guide, second ed. Cambridge University Press, Cambridge, United Kingdom, p. 681.
Potter, C.J., Schenk, C.J., Mercier, T.J., et al., 2019. Assessment of paleozoic shale-oil and shale-gas resources in the Tarim Basin of China: U.S. Geological survey fact sheet 2019–3011. https://doi.org/10.3133/fs20193011.
Sun, X.L., Chen, J.F., Liu, W.H., et al., 2004. Geochemical characteristics of cherts of lower cambrian in the Tarim Basin and its implication for environment. Petrol. Explor. Dev. 31 (3), 45–48 (in Chinese).
Sun, Y.G., Xu, S.P., Lu, H., et al., 2003. Source facies of the Paleozoic petroleum systems in the Tabei uplift, Tarim Basin, NW China: implications from aryl isoprenoids in crude oils. Org. Geochem. 34 (4), 629–634. https://doi.org/10.1016/S0146-6380(03)00063-9.
Sun, Z.Y., Chen, J., Wang, Q., et al., 2024. A quantitative analysis on thermochemical sulfate reduction products of two model compounds: implications for reaction mechanism and alteration process of hydrocarbons. Chem. Geol. 661, 122187. https://doi.org/10.1016/j.chemgeo.2024.122187.
Terken, J.M.J., Frewin, N.L., Indrelid, S.L., 2001. Petroleum systems of Oman: charge timing and risks. AAPG Bull. 85 (10), 1817–1845. https://doi.org/10.1306/8626D081-173B-11D7-8645000102C1865D.
Thompson, W., Peters, K.E., Magoon, L.B., et al., 2019. Identification of genetically distinct petroleum tribes in the Middle Magdalena Valley, Colombia. AAPG Bull. 103, 3003–3034. https://doi.org/10.1306/04101918107.
Tissot, B.P., Welte, D.H., 1984. Petroleum Formation and Occurrence. Springer-Verla, New York, p. 699.
Wang, H.Q., 2019. Source Rocks Sedimentary Environment and Hydrocarbon Generating Potential of the Lower Cambrian in Kalpin Thrust Belt. PHD thesis,. China University of Petroleum (Beijing) (in Chinese).
Wang, Q.H., Xu, Z.P., Zhang, R.H., et al., 2024. New fields, new types of hydrocarbon explorations and their resource potentials in Tarim Basin. Acta Petrol. Sin. 45 (1), 15–32. https://doi.org/10.7623/syxb202401002.
Wang, W.Y., Pang, X.Q., Wang, Y.P., 2022. Hydrocarbon expulsion model and resource potential evaluation of high-maturity marine source rocks in deep basins: example from the Ediacaran microbial dolomite in the Sichuan Basin, China. Petrol. Sci. 19 (6), 2618e2630. https://doi.org/10.1016/j.petsci.2022.11.018.
Wu, L., Zhu, G., Yan, L., et al., 2021. Late ediacaran to early cambrian tectonic–sedimentary controls on lower cambrian black shales in the Tarim Basin, Northwest China. Global Planet. Change 205, 103612. https://doi.org/10.1016/j.gloplacha.2021.103612.
Xiao, S., Narbonne, G.M., Zhou, C., et al., 2016. Towards an Ediacaran time scale: problems, protocols, and prospects. Episodes 39 (4), 540–555. https://doi.org/10.18814/epiiugs/2016/v39i4/103886.
Xiong, R., Zhou, J.G., Ni, X.F., et al., 2015. Distribution prediction of Lower Cambrian Yuertusi Formation source rocks and its sianificance to oil and gas exploration in the Tarim Basin. Nat. Gas. Ind. 35 (10), 49–56. https://doi.org/10.3787/j.issn.1000-0976.2015.10.006 (in Chinese).
Xu, B., Li, J.H., Xie, D., et al., 2011. Distribution of shale gas resources in CNPC exploration area. Special Oil Gas Reservoirs 18 (4), 1–6 (in Chinese).
Xue, N., 2021. The Development Model of the Cambrian Evaporite-Carbonate Rock Associated Source Rock in the Tarim Basin. PHD thesis, China University of Petroleum (Beijing) (in Chinese).
Yang, F.L., Wang, T.G., Li, M.J., 2016a. Geochemical study of Cambrian source rocks in the cratonic area of Tarim Basin, NW China. Nat. Gas Geosci. 27 (5), 861–872. https://doi.org/10.11764/j.issn.1672-1926.2016.05.0861 (in Chinese).
Yang, H.J., Chen, Y., Tian, J., et al., 2020a. Great discovery and its significance of ultra-deep oil and gas exploration in well Luntan-1 of the Tarim Basin. China Petrol. Explor 25 (2), 62–72. https://doi.org/10.3969/j.issn.1672-7703.2020.02.007 (in Chinese).
Yang, H.J., Yu, S., Zhang, H.Z., et al., 2020b. Geochemical characteristics of Lower Cambrian sources rocks from the deepest drilling of Well LT-1 and their significance to deep oil gas exploration of the Lower Paleozoic system in the Tarim Basin. Geochimica 49 (6), 666–682. https://doi.org/10.19700/j.0379-1726.2021.01.017 (in Chinese).
Yang, H.J., Zhu, G.Y., 2013. The condensate gas field geological characteristics and its formation mechanism in Tarim basin. Acta Petrol. Sin. 29 (9), 3233–3250 (in Chinese).
Yang, P., Liu, K.Y., Liu, J.L., et al., 2021. Petroleum charge history of deeply buried carbonate reservoirs in the Shuntuoguole low uplift, Tarim Basin. west China. Mar. Petrol. Geol. 128, 105063. https://doi.org/10.1016/j.marpetgeo.2021.105063.
Yang, Q.Y., Santosh, M., Collins, A.S., et al., 2016b. Microblock amalgamation in the north China craton: evidence from neoarchaean magmatic suite in the western margin of the Jiaoliao block. Gondwana Res. 31, 96–123. https://doi.org/10.1016/j.gr.2015.04.002.
Yang, X., Li, H.L., Yue, Y., et al., 2017. The strata and palaeo-geomorphology framework at the end of neoproterozoic and development mode of source rocks at

the beginning of Cambrian in Tarim Basin, China. J. Nat. Gas Geosci. 2 (5), 313–322. https://doi.org/10.1016/j.jnggs.2018.02.003.
Yi, S., Li, M., Guo, X., et al., 2019. Breakthrough direction of Cambrian pre-salt exploration fields in Tarim Basin. Acta Petrol. Sin. 40 (11), 1281–1295. https://doi.org/10.7623/syxb201911001.
Yuan, F.F., Yang, X.Z., Zhang, K., et al., 2024. Multiple geochronological evidences revealing oil charging and redistribution processes in the Tazhong-4 Oilfield, Tazhong Uplift (Tarim Basin): implications for quantitative reconstruction of petroleum accumulation history in superimposed basins. Mar. Petrol. Geol. 162, 106688. https://doi.org/10.1016/j.marpetgeo.2023.106688.
Yuan, H.W., Chen, S.P., Dai, K., et al., 2022. Distribution of cambrian source rock controlled by the inherited paleotopography on the precambrian basement in the Tarim Basin, NW China. Front. Earth Sci. 10, 864082. https://doi.org/10.3389/feart.2022.864082.
Zhang, K., Pan, W.Q., Su, J., et al., 2022. Distribution and hydrocarbon generation potential of the Nanhua-Cambrian source rocks in Tarim Basin. China Petrol. Explor 27 (4), 121–134. https://doi.org/10.3969/j.issn.1672-7703.2022.04.009 (in Chinese).
Zhang, S.C., Huang, H.P., Su, J., et al., 2014. Geochemistry of Paleozoic marine oils from the Tarim Basin, NW China. Part 4: paleobiodegradation and oil charge mixing. Org. Geochem. 67, 41–57. https://doi.org/10.1016/j.orggeochem.2013.12.008.
Zhang, Z.Y., Zhu, G.Y., Chen, W.Y., et al., 2024. Cryogenian-Cambrian tectono-sedimentary evolution, paleoclimate and environment effects, and formation of petroleum resources in the Tarim Block. Earth Sci. Rev. 248, 104632. https://doi.org/10.1016/j.earscirev.2023.104632.
Zhang, Z.Y., Zhu, G.Y., Zhang, Y.J., et al., 2018. The origin and accumulation of multi-phase reservoirs in the East Tabei uplift, Tarim Basin. China. Mar. Petrol. Geol. 98, 533–553. https://doi.org/10.1016/j.marpetgeo.2018.08.036.
Zhao, G.Y., Deng, Q., Zhang, H.Z., et al., 2023. Trace elements and stable isotopic geochemistry of two sedimentary sections in the lower Cambrian strata from the Tarim Basin, northwest China: implications for silicification and biological evolution. Mar. Petrol. Geol. 147, 105991. https://doi.org/10.1016/j.marpetgeo.2022.105991.
Zheng, D.Y., Pang, X.Q., Ma, X.H., et al., 2019. Hydrocarbon generation and expulsion characteristics of the source rocks in the third member of the Upper Triassic Xujiahe Formation and its effect on conventional and unconventional hydrocarbon resource potential in the Sichuan Basin. Mar. Petrol. Geol. 109, 175–192. https://doi.org/10.1016/j.marpetgeo.2019.06.014.
Zheng, J.C., Li, B., Liu, Y.L., et al., 2018. Study on thermal evolution modeling of lower Cambrian Yuertusi source rock. Tarim Basin. Petrol. Reservoir Eval. Devel. 8 (6), 7–12. https://doi.org/10.13809/j.cnki.cn32-1825/te.2018.06.002 (in Chinese).
Zhou, C.X., 2021. Study on Oil Source, Maturity and Charge Episodes of Marine Crude Oil in Cratonic Region of Tarim Basin. Ph.D. Thesis. Guangzhou Institute of Geochemistry, Chinese Academy of Sciences (in Chinese).
Zhou, J., Pang, X.Q., 2002. A method for calculating the quantity of petroleum generation and expulsion. Petrol. Explor. Dev. 29, 24–27. https://doi.org/10.1016/j.petrol.2019.02.059 (in Chinese).
Zhou, X.X., Lü, X.X., Zhu, G.Y., et al., 2019. Origin and formation of deep and superdeep strata gas from Gucheng-Shunnan Block of the Tarim Basin, NW China. J. Petrol. Sci. Eng. 177, 361–373. https://doi.org/10.1016/j.petrol.2019.02.059.
Zhu, G.Y., Chen, F.R., Wang, M., et al., 2018. Discovery of the lower Cambrian high-quality source rocks and deep oil and gas exploration potential in the Tarim Basin, China. AAPG Bull. 102 (10), 2123–2151. https://doi.org/10.1306/03141817183.
Zhu, G.Y., Hu, J.F., Chen, Y.Q., et al., 2022. Geochemical characteristics and formation environment of source rock of the lower cambrian Yuertusi Formation in well luntan 1 in Tarim Basin. Acta Geol. Sin. 96, 1–16. https://doi.org/10.19762/j.cnki.dizhixuebao.2022285 (in Chinese).
Zhu, G.Y., Li, T.T., Zhang, Z.Y., et al., 2020. Distribution and geodynamic setting of the late neoproterozoic– early cambrian hydrocarbon source rocks in the south China and tarim blocks. J. Asian Earth Sci. 201, 104504. https://doi.org/10.1016/j.jseaes.2020.104504.
Zhu, G.Y., Milkov, A.V., Li, J.F., et al., 2021. Deepest oil in Asia: characteristics of petroleum system in the Tarim basin, China. J. Petrol. Sci. Eng. 199, 108246. https://doi.org/10.1016/j.petrol.2020.108246.
Zhu, G.Y., Zhang, Z.Y., Milkov, A.V., et al., 2019a. Diamondoids as tracers of late gas charge in oil reservoirs: example from the Tazhong area, Tarim Basin, China. Fuel 253, 998e1017. https://doi.org/10.1016/j.fuel.2019.05.030.
Zhu, G.Y., Zhang, Z.Y., Zhou, X.X., et al., 2019b. The complexity, secondary geochemical process, genetic mechanism and distribution prediction of deep marine oil and gas in the Tarim Basin, China. Earth Sci. Rev. 198, 102930. https://doi.org/10.1016/j.earscirev.2019.102930.
Zhu, M.Y., Yang, A.H., Yuan, J.L., et al., 2019c. Cambrian integrative stratigraphy and timescale of China. Sci. China Earth Sci. 62, 25–60. https://doi.org/10.1007/s11430-017-9291-0 (in Chinese).
Zhu, X.X., Wang, Q.L., Chen, J., et al., 2019d. Distribution and carbon isotopic compositions of n-alkanes from the catalytic hydropyrolysis of the Cambrian kerogen in the Tarim Basin. Geochimica 48 (5), 447–457. https://doi.org/10.19700/j.0379-1726.2019.05.002 (in Chinese).